Check for updates

Plant Pathology

WILEY

ORIGINAL ARTICLE OPEN ACCESS

Inferring the Potential Spread of *Xylella fastidiosa* in Great Britain With a Mechanistic Landscape-Scale Model

Flavia Occhibove[1] | Daniel S. Chapman[2] | Steven M. White[1]

[1]UK Centre for Ecology & Hydrology, Wallingford, UK | [2]Biological and Environmental Sciences, University of Stirling, Stirling, UK

Correspondence: Flavia Occhibove (flavia.occhibove@gmail.com)

Received: 5 March 2026 | **Revised:** 18 September 2026 | **Accepted:** 15 October 2026

Keywords: emerging plant pathogen | mechanistic model | olive quick decline syndrome | *Philaenus spumarius* | SIR modelling | vector-borne plant disease

ABSTRACT

Xylella fastidiosa is an insect-vectored bacterial plant pathogen with a wide host range, impacting agricultural and horticultural industries. Once restricted to the Americas, severe European outbreaks have been discovered, causing substantial economic and social harm. Its potential entry, establishment and spread is therefore a major concern for *Xylella*-free locations, such as Great Britain. Yet, the potential dynamics and severity of outbreaks in novel environments remain poorly understood. We adapted a mechanistic landscape-scale spread model originally developed for olive quick decline syndrome in Puglia (Italy), incorporating local eco-epidemiological conditions and permissive host-availability assumptions to represent a 'worst-case scenario' for Great Britain. Our simulations indicated that, conditional upon successful entry and establishment, parts of Great Britain could support subsequent spread, but with slower spread and lower epidemic growth than in Puglia. Alternative dispersal scenarios produced qualitatively consistent results, with temperature limiting transmission and the spatial configuration of the potential-host landscape influencing epidemic size. Entry into southern and southeastern England resulted in potentially larger outbreaks, reflecting higher temperatures and less fragmented host patches. Under our assumptions, epidemics in Great Britain were longer with a greater proportion of asymptomatic infection than those in Puglia, potentially complicating early detection. The model represented an average host–pathogen interaction while not explicitly capturing variation among *X. fastidiosa* subspecies, strains, host competence or phenology. Our modelling approach can be adapted to other *X. fastidiosa*-free regions and refined as empirical data become available. The present investigation provides a framework for exploring *X. fastidiosa* spatiotemporal dynamics and evaluating disease mitigation strategies.

1 | Introduction

Xylella fastidiosa is a bacterial plant pathogen and the recognised agent of several severe and economically important diseases, including Pierce's disease of grapevines, citrus variegated chlorosis (CVC), olive quick decline syndrome (OQDS) and almond leaf scorch among others affecting perennial crops and landscape plants (Almeida and Nunney 2015). Originally restricted to the Americas, *X. fastidiosa* was discovered in Europe for the first time in 2013 causing the Puglia (Italy) OQDS outbreak (Loconsole et al. 2014; Saponari et al. 2013). Since then, outbreaks involving distinct *X. fastidiosa* strains and multiple host plants have been reported in other Italian regions as well as Spain, France and Portugal (EFSA et al. 2019), while isolated detections have occurred elsewhere in Europe and across the broader Mediterranean region (EPPO 2025). Diseases caused by *X. fastidiosa* can result in substantial environmental, economic and societal impacts in both endemic and newly affected areas (Gonçalves et al. 2014; Schneider et al. 2020). In California, Pierce's disease causes estimated annual direct losses of $104 million (Tumber et al. 2014). In Puglia, *X. fastidiosa* has killed

This is an open access article under the terms of the Creative Commons Attribution License, which permits use, distribution and reproduction in any medium, provided the original work is properly cited.

© 2026 The Author(s). *Plant Pathology* published by John Wiley & Sons Ltd on behalf of British Society for Plant Pathology.

millions of olive trees (*Olea europaea*), with cumulative regional damages approaching €3 billion and profound cultural and societal repercussions associated with landscape devastation (Calderoni et al. 2025; Colella et al. 2019). Left unmanaged, Mediterranean olive-producing countries are projected to collectively incur losses of several billion euros (Calderoni et al. 2025; Schneider et al. 2020).

Transmitted exclusively by xylem-sap feeding insects (Hemiptera, Auchenorrhyncha), *X. fastidiosa* is a xylem-limited gammaproteobacterium (*Xanthomonadaceae*) that multiplies within xylem vessels and can cause progressive plant desiccation (Rapicavoli et al. 2018). Its broad host range (> 650 species) encompasses interactions ranging from asymptomatic endophytism to severe disease (EFSA 2025), while its substantial genetic diversity and association with multiple vectors further contribute to variation in epidemiological behaviour (Rapicavoli et al. 2018; Occhibove et al. 2020). Symptoms are generally non-specific (e.g., leaf scorching, wilting) and may develop only after a prolonged period, ranging from 2 to 3 months in Pierce's disease to approximately 14 months in OQDS, depending on biotic and abiotic conditions (EFSA et al. 2019; Roper et al. 2019). Symptom development, severity and host mortality vary with environmental conditions, host species, host–pathogen interactions and pathogen genetics (Rapicavoli et al. 2018). Accordingly, the species comprises distinct subspecies—including *fastidiosa*, *pauca*, *multiplex* and *sandyi*—and sequence types with different host ranges, virulence and epidemiological characteristics, complicating predictions of its behaviour in newly affected ecosystems (Occhibove et al. 2020).

With no cure available, management relies primarily on vector control, removal of infected or susceptible hosts and the establishment of buffer zones (EFSA et al. 2019). The severity of outbreaks, uncertainty surrounding their potential distribution and the risk of human-mediated introduction have prompted EU emergency measures (EU 2015; and subsequent updates). Despite major advances in understanding pathogen biology, vector ecology and disease management (Purcell 2013; Rapicavoli et al. 2018; Roper et al. 2019; Saponari et al. 2019; Sicard et al. 2018), predicting *X. fastidiosa* emergence and subsequent dynamics in novel regions remains a critical challenge (Occhibove et al. 2020). Pathogen emergence involves sequential processes of entry (arrival), establishment (persistence and transmission), and subsequent landscape-scale spread. For *X. fastidiosa* pathosystems, these processes are shaped by complex interacting factors, including propagule pressure, host compatibility, environmental suitability, landscape structure, vector movement and climate (Occhibove et al. 2020).

Great Britain is currently *Xylella*-free, but the high volume of plant trade and presence of potentially suitable hosts and vectors, most notably *Philaenus spumarius*, might represent significant risk factors for entry and establishment of the pathogen (Defra 2020). Indeed, global trade networks have been recognised as a significant risk factor in the increasing rates of emergence of plant diseases (Chapman et al. 2017). However, although *X. fastidiosa* has been detected in several European countries and regions, sustained epidemics remain geographically restricted, indicating that plant-trade activity alone cannot explain its current distribution and that the determinants of successful establishment remain incompletely understood. This distinction is important when extrapolating from established European outbreaks to regions where *X. fastidiosa* has not yet become established. Because *X. fastidiosa* has not yet been detected in Great Britain, region-specific epidemiological data are lacking, particularly regarding host susceptibility, vector dispersal and transmission rates. These uncertainties are further compounded by the markedly different eco-epidemiological conditions in Great Britain compared with countries and regions where outbreaks have occurred (Occhibove et al. 2020). As highlighted by Occhibove et al. (2020), uncertainty in *Xylella* modelling arises not only from data gaps but also from structural non-transferability: parameters calibrated in Mediterranean systems implicitly incorporate climatic conditions, host phenology, vector ecology and landscape connectivity that may not apply under northern European conditions. Consequently, direct transfer of Italian or southern European parameter sets may produce biased estimates of invasion timing, epidemic velocity and spatial spread. In particular, where conditions in Great Britain are less favourable than those in the source system, such parameter transfer may underestimate the constraints on transmission and therefore result in conservative estimates of potential spread.

At present, the potential distribution of *X. fastidiosa* in Europe is largely inferred from correlative suitability distribution models (SDMs) (EFSA et al. 2019; Godefroid et al. 2019; Godefroid, Cruaud, et al. 2022; Schneider et al. 2020). However, SDMs do not explicitly represent dispersal mechanisms or spatiotemporal transmission dynamics, and climate-matching approaches may be unreliable when outbreaks have not yet occupied their full climatic niche (Briscoe et al. 2019). This may be particularly relevant when interpreting the current distribution of *X. fastidiosa* in Europe, where the absence of sustained outbreaks in some regions cannot be attributed to limited entry opportunities alone and may also reflect constraints on establishment and persistence under local climatic and ecological conditions. Alternative modelling approaches, including network analyses (Strona et al. 2017), mechanistic models (Kyrkou et al. 2018; Soubeyrand et al. 2018; White et al. 2017, 2020), Bayesian frameworks (Cendoya et al. 2020), hybrid models (Kottelenberg et al. 2021; Martinetti and Soubeyrand 2019) and reaction–diffusion-absorption models (Abboud et al. 2019), provide complementary approaches for representing the biological and spatial processes underlying *X. fastidiosa* spread. However, these models were developed for specific pathosystems and geographic contexts, and their parameterisations cannot necessarily be transferred directly to ecologically distinct locations such as Great Britain. Recent mechanistic modelling of Pierce's disease based on experimental data from European grapevine varieties showed that climatic constraints currently limit epidemic development across much of Europe, while future warming could expand areas suitable for pathogen establishment and spread (Giménez-Romero et al. 2022). These findings highlight the importance of mechanistic temperature responses when assessing *X. fastidiosa* establishment and spread.

In this context, mechanistic models provide a transparent framework for testing how differences in climate, vector phenology, host availability and landscape connectivity may fundamentally alter *X. fastidiosa* invasion dynamics. By

13653059, 2026, 6, Downloaded from https://bsppjournals.onlinelibrary.wiley.com/doi/10.1111/ppa.70322 by NICE, National Institute for Health and Care Excellence, Wiley Online Library on [18/11/2026]. See the Terms and Conditions (https://onlinelibrary.wiley.com/terms-and-conditions) on Wiley Online Library for rules of use; OA articles are governed by the applicable Creative Commons License

explaining the causal mechanisms that generate observed patterns, these types of models provide a more robust basis for extrapolation beyond the conditions under which they were originally tested (Yates et al. 2018). Hence, the objective of this study is to adapt an established mechanistic modelling framework to the environmental and landscape conditions of Great Britain to infer the pathogen's potential spread across the landscape, should it enter and become established with a suitable host–strain combination. The model should be interpreted as a mechanistic scenario framework rather than as a species-wide prediction of *X. fastidiosa* epidemiology. Available empirical evidence is insufficient to parameterise transmission, host susceptibility and disease progression across the range of host–pathogen combinations and environmental conditions potentially relevant to Great Britain. We therefore adapted the existing Puglian model using available data and a series of explicit assumptions, representing pathogen and host heterogeneity through an effective, average pathogen–host combination and adopting permissive host-availability assumptions to explore a 'worst-case scenario' of spread. Alternative environmental and dispersal scenarios were used to assess key factors affecting potential spread. This abstraction allows landscape-scale comparison of potential spread while necessarily omitting variation among *X. fastidiosa* subspecies and sequence types, host species and host–strain interactions.

Model outputs should therefore be interpreted as conditional estimates of potential outbreak extent under the specified assumptions, rather than as estimates of the probability of entry or establishment in Great Britain. Specifically, we address the following policy-relevant questions: (i) Conditional on a successful entry of *X. fastidiosa* and local establishment, are British eco-epidemiological conditions conducive to subsequent landscape-scale spread of *X. fastidiosa*? (ii) If so, where would pathogen entry be most likely to trigger a larger outbreak? (iii) What is the potential severity of such outbreaks, and can spatial risk factors be identified that characterise locations with higher outbreak potential? To answer these questions, we adapted the mechanistic model originally developed for the OQDS outbreak in Puglia by White et al. (2020) and Chapman et al. (2025) to local eco-epidemiological conditions. We further designed a suite of biologically informed scenarios to compare potential spread between Great Britain and Puglia and across British regions, which differ, among other factors, in the spatial configuration of host plants.

2 | Materials and Methods

The mechanistic modelling approach in this study was adapted from White et al. (2020) (which was built upon White et al. 2017) and Chapman et al. (2025) to account for the different biotic and abiotic conditions in Great Britain relative to Puglia. In particular, we adapted the representation of susceptible host distribution, climate and vector dispersal, which were expected to be key determinants of the rate and spatial extent of pathogen spread. The spatially explicit model represents transmission following an infected entry through susceptible, asymptomatic, symptomatic and desiccated host compartments, and simulates both within-cell infection and between-cell spread as a function of temperature, host availability and dispersal. We used biologically informed scenarios, including entry of the pathogen at multiple locations, to explore how these factors influence potential outbreak size and spatial extent across Great Britain.

The model is designed to assess conditional post-establishment spread and therefore does not estimate the probability of pathogen entry or establishment, propagule pressure or trade-mediated entry pathways. Similarly, because the available empirical evidence is insufficient to parameterise these processes consistently across the range of host–pathogen combinations and environmental conditions relevant to Great Britain, the model does not explicitly represent individual *X. fastidiosa* subspecies, species-specific host competence, host phenology, hourly temperature variation or winter curing. Winter curing (or cold curing), best documented in grapevines affected by Pierce's disease, is the reduction or elimination of the infection in hosts following exposure to low winter temperatures, potentially resulting in recovery (Feil and Purcell 2001). Instead, pathogen and host heterogeneity are represented through an effective average host–pathogen interaction, while environmental and dispersal uncertainty is explored through alternative scenarios. Thus, model outputs represent potential spread under specified assumptions rather than predictions of the probability of entry or establishment.

2.1 | Definition of Susceptible Population

Detailed information on the occurrence, abundance and epidemiological competence of individual *X. fastidiosa* host species in Great Britain is lacking. We therefore adopted a conservative 'worst-case scenario' approach to represent the spatial distribution and density of the potential host population across the landscape. Unlike Puglia, where the epidemic is strongly associated with a single highly susceptible host, *O. europaea*, the British landscape contains a diverse assemblage of potential hosts, including ornamental plants, amenity trees and native shrubs. Several plant species that are widespread in Great Britain, including *Lavandula*, *Rosmarinus*, *Prunus*, *Quercus*, *Acer* and *Polygala* spp., are recognised hosts of *X. fastidiosa* in continental Europe and are associated with strains established in southern Europe (EFSA 2025).

Because the host–strain combination involved in a potential future British introduction cannot be predicted, we represented the system using an effective average host–pathogen interaction, rather than assuming a specific host species or *X. fastidiosa* subspecies. The potential-host landscape therefore represents host availability rather than epidemiologically equivalent hosts. We do not assume that all included species are equally susceptible or competent for transmission: some may contribute substantially to transmission, whereas others may function primarily as epidemiological sinks. However, the available species- and strain-specific competence data are insufficient to parameterise these differences for Great Britain, and they are therefore incorporated implicitly within the effective average host parameterisation. The resulting host-density layer should not be interpreted as a measure of infectious or epidemiologically competent host abundance. The model also does not explicitly distinguish between evergreen

13653039, 2026, 6, Downloaded from https://bsppjournals.onlinelibrary.wiley.com/doi/10.1111/ppa.70322 by NICE, National Institute for Health and Care Excellence, Wiley Online Library on [18/11/2026]. See the Terms and Conditions (https://onlinelibrary.wiley.com/terms-and-conditions) on Wiley Online Library for rules of use; OA articles are governed by the applicable Creative Commons License

and deciduous hosts or represent the annual dormancy of hosts and associated changes in infection dynamics. Consequently, the susceptible population is treated as a spatially distributed, temporally available potential host population throughout the simulation period.

Potential *X. fastidiosa* host areas were identified by cross-referencing, at the finest taxonomic resolution available, the updated database of susceptible hosts (EFSA 2025) with PLANTATT, the database of British native and non-native plant attributes (Hill et al. 2004). This approach enabled the exclusion of habitats where susceptible hosts were absent. Among the hosts listed by EFSA (2025), only semi-woody and woody species were retained for analysis. Herbaceous hosts were excluded due to the impracticality of reliably estimating their density, and because most documented European outbreaks have occurred on woody species. Host distribution was mapped using high-resolution (25 m) land cover maps (Rowland et al. 2015), matching land cover classes with the habitats in which the potential British hosts occurred (from the classification in Hill et al. 2004). The included land cover classes (from Rowland et al. 2015) were broadleaved woodland; arable and horticulture; fen, marsh and swamp; heather; bog; supra-littoral rock; supra-littoral sediment; saltmarsh; urban; and suburban. Arable land with non-susceptible crops and urban areas with no green spaces (or green spaces with non-susceptible hosts) were excluded using the UKCEH Crop Map (UKCEH 2016) and the OS Open Greenspace Map (https://www.ordnancesurvey.co.uk/products/os-open-greenspace; Crown copyright and database right 2020), respectively. Total susceptible population density (N) of the identified susceptible areas was estimated according to Crowther et al. (2015), which estimates tree density of different biomes at the global scale (Figure S2b). This was resampled at the 200 × 200 m resolution, that is, model basic spatial unit, and adjusted by the percentage of vegetation cover estimated using a vegetation index from satellite data, the normalised difference vegetation index (NDVI), a remote-sensing index derived from red and near-infrared reflectance that indicates vegetation greenness and photosynthetic activity (2008–2018 average NDVI from MOD13Q1 16-day) (Figure S2c). The final simulation landscape consisted of susceptible grid cells organised into patches of varying size and connectivity, reflecting the exclusion of areas where susceptible host species were assumed to be absent (Figure S3a).

2.2 | Transmission Dynamics in Great Britain—Within-Cell Transmission

The transmission dynamics comprised a compartmental short-distance transmission, within 200 × 200 m grid cells (basic spatial unit), and a stochastic long-distance spread, representing the dispersal between grid cells, at a yearly temporal scale to correspond with vector dispersal patterns and seasonality (IPSP-CNR et al. 2019) (Figure 1). The short-distance model (within-cell transmission) was an adaptation from White et al. (2020), which was developed for the OQDS in Puglia and represented the local infection growth within a grid cell (i.e., progression of disease within the grid cell as a fraction of trees infected). They developed a variation of the classic compartmental SEIR model (Allen 1994), using a Bayesian framework to fit it to disease progression data from experimental plots of infected olive trees. Building on this approach, our deterministic population-level compartmental model (Figure 1a) included four stages: susceptible (S), infected asymptomatic (A), infected symptomatic (I), and desiccated (D) (SAID), described by the equations below (Equations 1–7) (see Table 1 for full notation). Infected individuals first underwent an incubation period during which they were infected but asymptomatic. Symptomatic (I) trees remained in this stage for τ years (desiccation delay), so that the transition from infected to desiccated was held for τ years. We denoted the τth compartment of symptomatic sojournment by I_t^r. The total proportion of infected symptomatic trees was given by:

$$I_t = \sum_{j=1}^{\tau+1} I_t^j$$

The epidemiological dynamics at population level were given by

$$S_{t+1} = (1-\alpha_t)S_t \tag{1}$$

$$A_{t+1} = \alpha_t S_t + (1-\sigma)A_t \tag{2}$$

$$I_{t+1}^1 = \sigma A_t \tag{3}$$

$$I_{t+1}^2 = I_t^1 \tag{4}$$

$$\vdots$$

$$I_{t+1}^r = I_t^{\tau-1} \tag{5}$$

$$I_{t+1}^{\tau+1} = I_t^\tau + (1-\gamma)I_t^{\tau+1} \tag{6}$$

$$D_{t+1} = D_t + \gamma I_t \tag{7}$$

The total host population did not change over time:

$$N_{t+1} = S_t + A_t + I_t + D_t = N_t, \text{thus } N_t = N, \text{constant}, \forall t.$$

The time-dependent individual annual probability of being infected, infection rate

$$\alpha_t = e^{-\beta \frac{b_A A_t + I_t + b_D D_t}{N_t}} \tag{8}$$

was developed to account for British lower temperature compared to Puglia (Equation 9, Table 1, and Figure S2a). *X. fastidiosa* growth and consequent within-plant colonisation have been observed to be limited by temperature (Feil and Purcell 2001), as well as its spread rate because of temperature-dependent bacterial survival rate (Gould and Lashomb 2005; Sicard et al. 2018) and the preference of vectors for milder temperatures (Cornara et al. 2019). Similarly to White et al. (2020), infected asymptomatic (A) and desiccated (D) individuals were partially infectious compared to symptomatics (I).

The transmission rate

$$\beta = C\beta_P \tag{9}$$

13653059, 2026, 6, Downloaded from https://bsppjournals.onlinelibrary.wiley.com/doi/10.1111/ppa.70322 by NICE, National Institute for Health and Care Excellence, Wiley Online Library on [18/11/2026]. See the Terms and Conditions (https://onlinelibrary.wiley.com/terms-and-conditions) on Wiley Online Library for rules of use; OA articles are governed by the applicable Creative Commons License

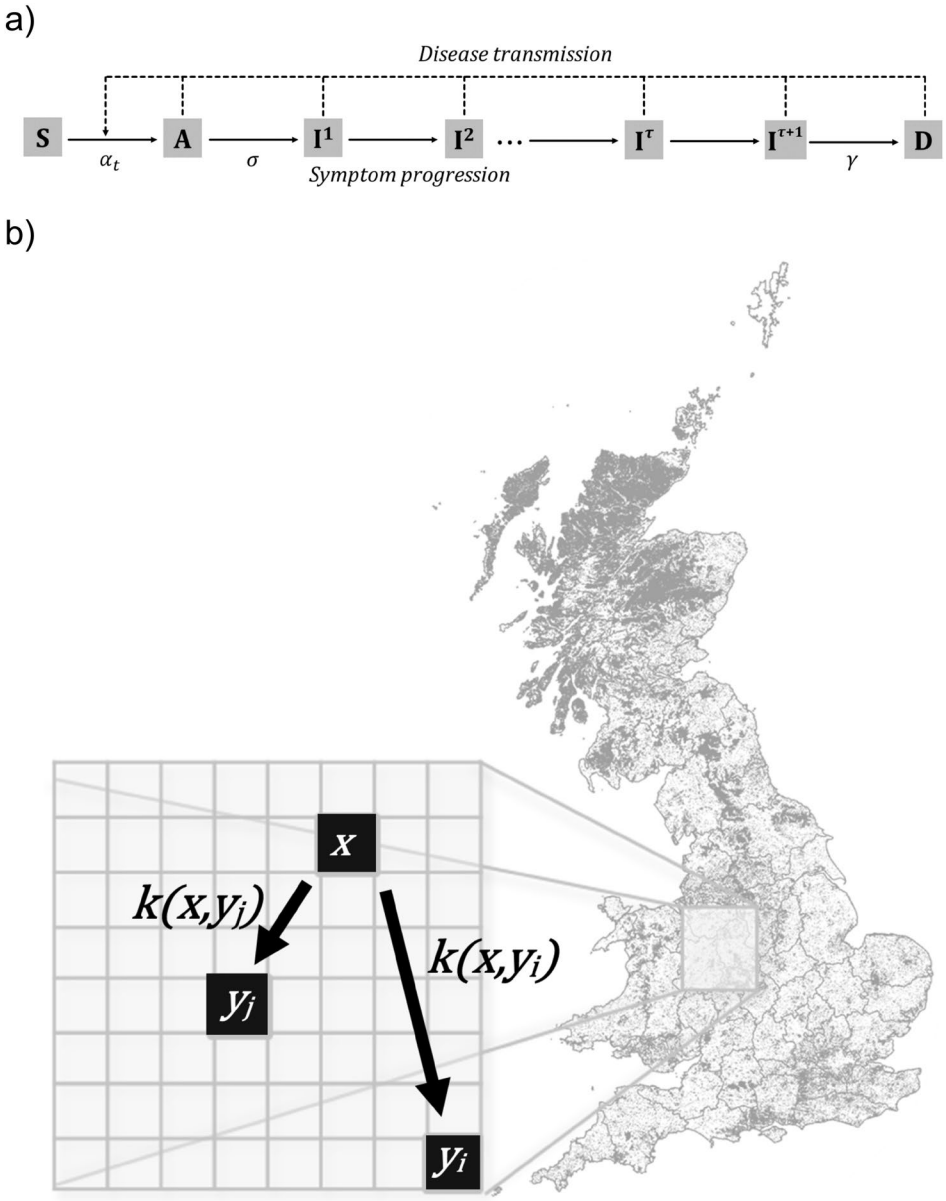

FIGURE 1 | (a) Deterministic compartmental model developed for Great Britain for *Xylella fastidiosa*. Boxes represent epidemiological compartments; arrows indicate movement between compartments with corresponding rates (see Table 1 for parameters and notation). σ, rate of progression from asymptomatic to symptomatic infection; α_t, time-dependent infection rate; γ, rate of progression from symptomatic infection to desiccation; A, infected asymptomatic; D, desiccated; I, infected symptomatic; S, susceptible. The model is identical to the generalised full epidemiological $SI_AI_SI_D$ model in White et al. (2020) when $C=1$, $w_I=1$, and $w_D=1$. (b) Visual representation of long-distance dispersal. The grid represents a subsection of the British landscape divided into 200×200 m grid cells. Grey cells: susceptible uninfected; black cells: infected, with transitions to asymptomatic, symptomatic, or desiccated according to deterministic model rates. Arrows indicate dispersal direction according to the kernel: $k(x,y)$.

was estimated by scaling the Puglian transmission rate β_P (Table 1) by a British-specific temperature suitability factor C. This factor C accounts for the effect of local temperature on bacterial growth and therefore on potential transmission relative to the conditions under which the original Puglian model was parameterised.

The temperature suitability function was derived from in vitro temperature-dependent growth experiments involving 12 *X. fastidiosa* strains representing four subspecies (*fastidiosa*, *multiplex*, *pauca* and *sandyi*) (Román-Écija et al. 2026) (Table 1 and Figure S1). A polynomial curve was fitted to the growth data to describe the in vitro growth response of an average *X. fastidiosa* strain across a temperature range of 4°C–39°C. The growth optimum corresponded to the average summer temperature in Puglia. The resulting temperature suitability function was $C = 0.00016T_s^3 - 0.00317T_s^2 + 0.02062\,T_s - 0.04049$. The factor ranged from 1, representing maximum suitability at Puglia's average summer temperature, to 0, when no growth was observed. The mean response across all strains was used to represent an effective species-level temperature response because the identity of a future entry of *X. fastidiosa* into Great Britain is unknown. This approach necessarily averages subspecies- and strain-specific differences in thermal responses and should not be interpreted as implying equivalent thermal suitability or establishment

13653059, 2026, 6, Downloaded from https://bsppjournals.onlinelibrary.wiley.com/doi/10.1111/ppa.70322 by NICE, National Institute for Health and Care Excellence, Wiley Online Library on [18/11/2026]. See the Terms and Conditions (https://onlinelibrary.wiley.com/terms-and-conditions) on Wiley Online Library for rules of use; OA articles are governed by the applicable Creative Commons License

TABLE 1 | Eco-epidemiological parameters used in the SAID model for *Xylella fastidiosa* in Great Britain, including their definitions and methods of estimation.

Parameter	Parameter name/meaning	Estimation method	Value/ range
β_p	Effective contact rate for infected individuals	Transmission rate from White et al. (2020)	17.88
b_A	Infectivity of asymptomatic individuals, relative to fully infectious individuals	From White et al. (2020)	0.01
b_D	Infectivity of desiccated individuals, relative to fully infectious individuals	From White et al. (2020)	0.503
C	Temperature scaling factor	Coefficient estimated from in vitro temperature-dependent growth curves of *Xylella fastidiosa* strains (all subspecies and strains combined) and the British average summer temperature range T_s (Robinson et al. 2020), assuming the Puglia average summer temperature T as the maximum growth reference (Román-Écija et al. 2026) (Figure S1). The coefficient does not account for hourly temperature fluctuations or overwintering. $C = \left(0.00016T_s^3 - 0.00317\,T_s^2 + 0.02062\,T_s - 0.04049\right)$	0–0.16
T_a	Mean duration of the symptomless period (years)	From White et al. (2020)	1.19
T_d	Mean time to desiccation (years)	From White et al. (2020)	1.36
τ	Desiccation delay parameter (years)	From White et al. (2020)	3
w_I	Environmental scaling factor affecting incubation period	Climatic water deficit values from 1980 to 2015 (Abatzoglou et al. 2018) showed that Great Britain has substantially lower deficits than Puglia (Table S1). This supported the assumption of a longer asymptomatic period in Britain due to reduced water stress (McElrone et al. 2001; Choi et al. 2013; de Pascali et al. 2019; Saponari et al. 2019). Landscape heterogeneity and variability in host susceptibility were also assumed, based on the simulation scale and the 'worst-case scenario' estimation of susceptible populations (see section 2.1 Definition of Susceptible Population). To represent these environmental differences affecting the incubation period, values from 0 to 5 were assigned, with 1 corresponding to Puglia conditions. Values <1 indicated shorter asymptomatic periods (e.g., 0 = no incubation; 1 = same as Puglia), while values >1 indicated prolonged incubation (e.g., 2 = twofold increase). Upper limits were chosen to maintain compatibility with host-plant life cycles. Subject to parameter exploration. Not host-specific.	0–5
w_D	Environmental scaling factor affecting time to desiccation	In line with the assumptions applied to the incubation period, a reduced desiccation rate was therefore assumed for Great Britain. To represent these environmental effects on the time to desiccation, scaling values from 0 to 5 were explored, with 1 corresponding to Puglia conditions. Values <1 indicated faster progression to desiccation (e.g., 0 = zero time to desiccation, 1 = same as Puglia), whereas values >1 indicated slower progression to desiccation (e.g., 2 = twofold increase in time to desiccation), while maintaining consistency with host plant life cycles. Subject to parameter exploration. Not host-specific.	0–5

(Continues)

13653059, 2026, 6, Downloaded from https://bsppjournals.onlinelibrary.wiley.com/doi/10.1111/ppa.70322 by NICE, National Institute for Health and Care Excellence, Wiley Online Library on [18/11/2026]. See the Terms and Conditions (https://onlinelibrary.wiley.com/terms-and-conditions) on Wiley Online Library for rules of use; OA articles are governed by the applicable Creative Commons License

TABLE 1 | (Continued)

Parameter	Parameter name/meaning	Estimation method	Value/ range
θ	Scale parameter of dispersal kernel	From Chapman et al. (2025)	10^{-6}
k_l	Long-distance dispersal (km)	From Chapman et al. (2025)	5.92
k_s	Short-distance dispersal (km)	From Chapman et al. (2025)	0.32
k_{sGB}	Short-distance dispersal (km)	Assumed half of the value from Chapman et al. (2025) due to lower vector dispersal distances found in Great Britain (Hogenhout et al. 2022)	0.16

Note: Values are provided where available; for parameters explored via sensitivity analysis, the evaluated ranges are indicated. SAID: susceptible (S), infected asymptomatic (A), infected symptomatic (I), and desiccated (D).

potential among subspecies. Great Britain-specific average summer temperatures (Robinson et al. 2020) were then applied to the fitted function to estimate C for each grid cell, thereby capturing spatial variation in temperature suitability across Great Britain (Figure S2a). The resulting transmission rate was consequently lower than the Puglian reference rate in areas where British temperatures were less favourable for bacterial growth. This formulation, based on mean summer temperature, did not explicitly account for hourly or diurnal temperature variation, short-duration cold events, or cumulative thermal exposure, for which experimental data are currently insufficient to quantify their effects on transmission across relevant host–pathogen combinations. However, mean temperature was selected as one of the bioclimatic variables most strongly associated with *X. fastidiosa* growth under experimental conditions and climatic suitability in SDMs (EFSA et al. 2019). The temperature suitability factor therefore represented the potential effect of temperature on bacterial growth and transmission and should not be interpreted as a threshold for successful pathogen establishment.

White et al. (2020) and Chapman et al. (2025) did not explicitly model vector population, and the influence of the vector was implicit in their infection rate. Preliminary investigations on *X. fastidiosa* vectors in Great Britain revealed that adult densities were comparable to those in Puglia and other European countries (Chapman et al. 2022; Hogenhout et al. 2022), so we did not further modify the transmission rate to reflect different vector densities.

Individual annual transition probabilities for infected asymptomatic individuals becoming symptomatic (incubation or asymptomatic period)

$$\sigma = 1 - e^{-\frac{1}{T_A}} \tag{10}$$

and annual mortality of infected symptomatic individuals, after τ years in the symptomatic compartment

$$\gamma = 1 - e^{-\frac{1}{T_D}} \tag{11}$$

were adapted from White et al. (2020), so that the asymptomatic period and the time to desiccation were dependent upon the environmental scaling factors, w_I and w_D respectively (Equations 12 and 13).

$$T_A = w_I T_a \tag{12}$$

$$T_D = w_D T_d \tag{13}$$

These parameters represented overall differences in environmental conditions assumed to affect disease progression in Great Britain compared with Puglia (Table 1), including ecological factors such as landscape heterogeneity and reduced climatic water deficit in Great Britain compared to Puglia (Table S1). While the model of White et al. (2020) specifically described the transmission of *X. fastidiosa* subsp. *pauca* in olives in Puglia, we considered an average host–bacterium strain combination to reflect uncertainty regarding the identity of a potential introduction and the greater heterogeneity of potential hosts in Great Britain. The parameters derived from the Puglian olive pathosystem were therefore used here as effective epidemiological durations rather than as host-independent estimates. The mean symptomless period of 1.19 years (Table 1) was retained from White et al. (2020) and applied as a continuous epidemiological duration, scaled to local environmental conditions, rather than being reset according to host phenology. Consequently, the model does not explicitly represent seasonal dormancy or the annual resetting of asymptomatic infection in deciduous hosts.

Moreover, the lower climatic water deficit in Britain compared to Puglia (Table S1) most likely reduced the exposure of British vegetation to hydric stress (Dilts et al. 2015; Vicente-Serrano et al. 2013), which has been observed to influence symptom development and desiccation (Choi et al. 2013; de Pascali et al. 2019; McElrone et al. 2001; Saponari et al. 2019). Nevertheless, no experimental data were available to link landscape heterogeneity or climatic water deficit, and consequently plant hydric stress, to disease progression times. Therefore, we defined a plausible range of values for the environmental scaling factors (w_I and w_D) and performed parameter exploration (see the Model parameterisation Section 2.4 and Figure 2).

2.3 | Transmission Dynamics in Great Britain—Between-Cell Transmission

The model spatial component was based on *X. fastidiosa* vector dispersal mechanisms (i.e., local dispersal by flight locally or by wind, or long-distance dispersal through unintentional hitchhiking on human vehicles) (Chapman et al. 2025). The distribution of diseased hosts (i.e., olive trees) in Puglia suggested a degree of local spread in conjunction with long-distance dispersal, resulting in a strong clustering of outbreak locations (Chapman et al. 2025). Thus, similarly to Chapman et al. (2025),

13653059, 2026, 6, Downloaded from https://bsppjournals.onlinelibrary.wiley.com/doi/10.1111/ppa.70322 by NICE, National Institute for Health and Care Excellence, Wiley Online Library on [18/11/2026]. See the Terms and Conditions (https://onlinelibrary.wiley.com/terms-and-conditions) on Wiley Online Library for rules of use; OA articles are governed by the applicable Creative Commons License

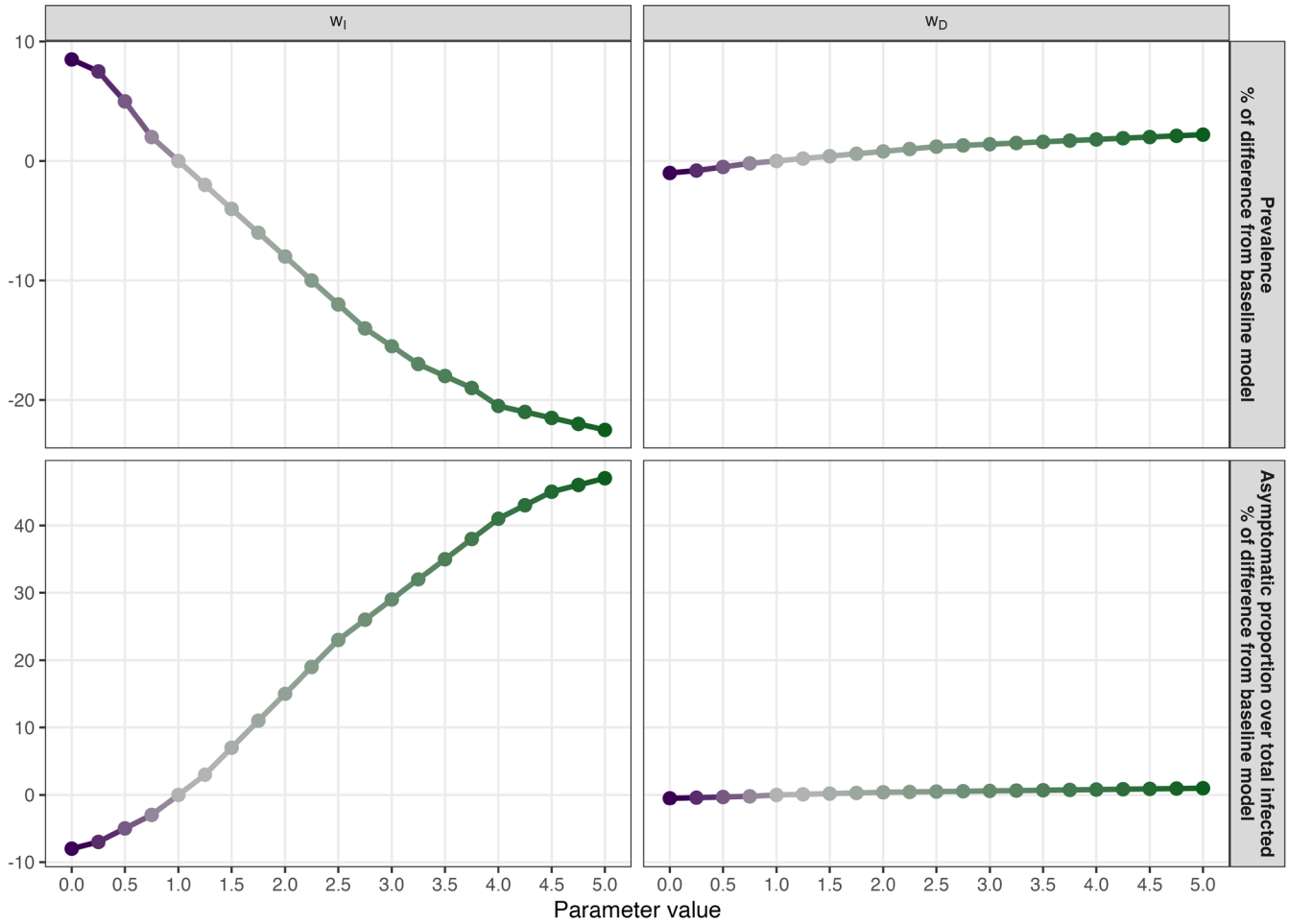

FIGURE 2 | Parameter exploration for the SAID (susceptible-infected asymptomatic-infected symptomatic-desiccated) model for *Xylella fastidiosa* for Great Britain. The plots show the percentage change in infection prevalence (upper panels) and proportion of asymptomatic individuals over total infected (lower panels), for environmental scaling factors w_I and w_D (on the *x*-axis) compared to the baseline Puglia model ($\beta = \beta_p = 17.88$; $\tau = 3$; $b_A = 0.01$; $b_D = 0.50$; $w_I = 1$; $w_D = 1$) (see Table 1 for notation). Simulations were performed over 16 years.

we assumed that stochastic long-distance spread was represented by the sum of the short-distance and long-distance kernels, reflecting vector short-distance and long-distance dispersal respectively (Figure 1b), which resulted in the following kernel (parameters listed in Table 1)

$$k(x,y) = (1-\theta)e^{\frac{(x-y)^2}{-2k_s^2}} + \theta e^{\frac{|x-y|}{-k_l}}. \quad (14)$$

We assumed isotropic stochastic dispersal, as Chapman et al. (2025) found insufficient evidence to support anisotropic dispersal mediated by road networks or prevailing winds. A weighted probability to get infected was assigned to each uninfected but susceptible grid cell according to the kernel distribution (i.e., the distance from an infected cell), so that the long-distance spread events depended upon the distribution of the susceptible cells over the landscape (Chapman et al. 2025).

2.4 | Model Parameterisation

Parameter values, sources, and estimation methodology are listed in Table 1. The parameters used to adapt the model to British local environmental conditions were estimated from mechanistic experiments (see Temperature scaling factor, *C*) and from empirical observations in Great Britain (see Short-distance dispersal, k_{sGB}). In contrast, parameter exploration was performed for the environmental scaling factors (w_I and w_D), as no mechanistic experiments or empirical observations specific to Great Britain were available for their estimation. The chosen parameter ranges were designed to test model behaviour under variation and to ensure that the epidemic timeline remained compatible with the host plant life cycle. We compared prevalence and the total proportion of symptomless plants, relevant for disease management, obtained under different parameter values with those from a model simulating Puglia conditions (baseline values in Figure 2). Parameters were varied one at a time, while all others were held at baseline values reported in Table 1. Infection was introduced as a single asymptomatic individual in each susceptible grid cell. For scenario simulations, we selected $w_I = w_D = 3$, to reflect slower symptom expression and longer desiccation times compared to Puglia; this value corresponded to the ratio of the maximum Puglia climatic water deficit to that of Great Britain (see Tables S1 and 2).

2.5 | Simulation Scenarios

All simulations were initiated by introducing a single infected individual into a susceptible location. The model therefore

13653059, 2026, 6, Downloaded from https://bsppjournals.onlinelibrary.wiley.com/doi/10.1111/ppa.70322 by NICE, National Institute for Health and Care Excellence, Wiley Online Library on [18/11/2026]. See the Terms and Conditions (https://onlinelibrary.wiley.com/terms-and-conditions) on Wiley Online Library for rules of use; OA articles are governed by the applicable Creative Commons License

TABLE 2 | Epidemiological scenarios simulated to represent plausible eco-epidemiological settings for *Xylella fastidiosa* in Great Britain.

Scenario	Infection rate (β)	Environmental scaling factor—incubation period (w_I)	Environmental scaling factor—time to desiccation (w_D)	Dispersal kernel	Justification
Puglia	$\beta = \beta_p$	$w_I = 1$	$w_D = 1$	$k_l + k_s$ (Chapman et al. 2025)	Baseline parameterisation from White et al. (2020) and Chapman et al. (2025), representing OQDS dynamics in Puglia.
GB_FullDispersal	$\beta = C\beta_p$	$w_I = 3$	$w_D = 3$	$k_l + k_s$ (Chapman et al. 2025)	The transmission rate in GB is considered to be lower compared to the transmission rate reported in White et al. (2020), as it has been demonstrated that *Xylella fastidiosa* growth is limited by temperature (Román-Écija et al. 2026). Longer incubation and symptomatic periods reflect lower climatic water deficit in GB (asymptomatic individuals took three times longer to develop symptoms and symptomatic individuals were assumed to take three times longer to desiccate than in Puglia). Full dispersal retained to test climate-only effects
GB_Short	$\beta = C\beta_p$	$w_I = 3$	$w_D = 3$	k_s (Chapman et al. 2025)	As above for climate scaling and disease progression, but assuming only short-distance dispersal to reflect reduced vector-mediated long-range movement in Britain (Chapman et al. 2022; Hogenhout et al. 2022)
GB_ShortReduced	$\beta = C\beta_p$	$w_I = 3$	$w_D = 3$	k_{sGB} (half k_s from Chapman et al. 2025)	As above, with further reduced short-distance dispersal based on British vector movement estimates (Hogenhout et al. 2022), to explore lower-mobility conditions.

Note: Parameter values not specified in this table were set according to Table 1.
Abbreviation: OQDS, olive quick decline syndrome.

13653059, 2026, 6, Downloaded from https://bsppjournals.onlinelibrary.wiley.com/doi/10.1111/ppa.70322 by NICE, National Institute for Health and Care Excellence, Wiley Online Library on [18/11/2026]. See the Terms and Conditions (https://onlinelibrary.wiley.com/terms-and-conditions) on Wiley Online Library for rules of use; OA articles are governed by the applicable Creative Commons License

evaluated potential outbreak spread conditional on successful entry to Great Britain and did not estimate the probability of entry or establishment. Due to uncertainties regarding vector dispersal abilities in Great Britain, three scenarios—GB_FullDispersal, GB_Short, and GB_ShortReduced—were simulated to evaluate the impact of varying vector dispersal distances on *X. fastidiosa* spread across the heterogeneous landscape of susceptible hosts. Each scenario employed a different dispersal kernel, as detailed in Table 2. GB_FullDispersal represented dispersal similar to Puglia, where the final dispersal distance was calculated as the sum of short- and long-distance kernels (Equation 14).

Because recent population genetic studies provided little evidence of long-distance dispersal by potential *X. fastidiosa* vectors in Great Britain (Hogenhout et al. 2022), we hypothesised two additional scenarios incorporating only short-distance dispersal (setting $\theta = 0$ in Equation 14). Of these, GB_Short used the short-distance parameter value observed in Puglia (from Chapman et al. 2025), while in GB_ShortReduced this value was halved, reflecting experimental evidence that British vectors disperse less than their Puglian counterparts (Chapman et al. 2022; Hogenhout et al. 2022). Because spread in the model was stochastic, each scenario was simulated 152,923 times with different locations of entry, corresponding to 10% of all susceptible grid cells. Initial points of entry were selected using stratified random sampling by county to avoid bias due to differences in county size (susceptible areas and seeding points are shown in Figure S3).

A single simulation involved a single infection entry, from which the pathogen spread through the landscape via the dispersal kernel (an example of spatial spread for a single simulation is shown in Figure S4). Model outputs for each scenario were summarised as county-level averages (i.e., British ceremonial counties), with values indexed according to the county of pathogen introduction. Counties were selected as the reporting spatial unit because they provide an administratively meaningful scale for plant health management and surveillance, facilitate visualisation and communication of spatial patterns, and allow robust aggregation of stochastic simulation outcomes within comparable geographic units. While spread was simulated on a regular grid, summarising results at the county level enabled the averaging of stochastic realisations and supported direct interpretation for policy and management applications. Simulations were conducted in R (R Core Team 2024) over a 16-year period to capture the extended disease progression (EFSA et al. 2019).

2.6 | Analysis of Landscape Metrics of Infected Area

To test whether outbreak severity was associated with specific landscape configurations, we analysed the relationship between the spatial structure of susceptible hosts and the extent of simulated epidemics. In particular, we assessed whether differences in host patch size, connectivity and aggregation were linked to variation in outbreak severity, measured as the total number of infected cells.

At the end of each simulation, landscape metrics were estimated for the resulting total infected area, which was defined by the radius from the seeding location to the furthest infected cell. These metrics, selected according to the available relevant literature (Condeso and Meentemeyer 2007) were estimated with the *landscapemetrics* package in R (Hesselbarth et al. 2019). These included 'area and edge' metrics (mean area of patches in hectares, standard deviation of patch area, coefficient of variation of patch area, total susceptible area in hectares), and 'aggregation' metrics (patch cohesion, mean Euclidean nearest-neighbour distance (ENN) between patches in metres, ENN standard deviation, ENN coefficient of variation, number of patches, patch density as number of patches per 100 ha) (Figure S5). Because the model was stochastic, each simulation produced a different infected area and a corresponding set of landscape metric values. These were averaged by scenario and screened for collinearity to avoid concurvity, using Pearson's correlation with $r = 0.75$ as the exclusion threshold. For each of the three scenarios, we fitted generalised additive models (GAMs) for the total number of infected cells as a function of the uncorrelated 'area and edge' and 'aggregation' metrics: mean patch area (PA), coefficient of variation of patch area (PA_CV), mean ENN between patches, ENN coefficient of variation (ENN_CV), and patch density (PD). Because the data were over dispersed, a negative binomial distribution was used. All analyses were performed in R (R Core Team 2024) using the *gam* function from the *mgcv* package (v. 1.8-36; Wood 2011).

3 | Results

3.1 | Parameter Exploration

Results of the w_I and w_D parameter exploration showed that, relative to the Puglian baseline (parameter value = 1), increasing w_I and w_D above 1 produced slower simulated disease progression in Great Britain, characterised by a prolonged asymptomatic incubation phase and extended survival of symptomatic hosts. This was associated with lower overall infection prevalence and, particularly for w_I, a greater proportion of asymptomatic individuals among the total infected population (Figure 2). In this parameter exploration, only w_I and w_D were varied, whereas the environmental transmission scaling factor, C, was not independently explored and was held at its Puglian baseline. C was instead incorporated into the subsequent landscape simulations, where it varied spatially among cells according to mean summer temperature.

To quantify the magnitude of the effects of parameter variation, increasing *wI* resulted in a progressive decrease in prevalence, reaching approximately 22%–23% below the baseline at $w_I = 5$. Over the same range, the proportion of asymptomatic individuals increased to approximately 46%–47% above the baseline at $w_I = 5$. The strongest changes occurred around the baseline value, with progressively smaller changes towards the upper and lower bounds of the explored range. By contrast, w_D had a substantially smaller effect: across the same parameter range, prevalence varied by approximately −1% to +2% relative to the baseline, while the proportion of asymptomatic individuals varied even less in either direction (Figure 2). These results indicate that model outputs were considerably more sensitive to the duration of the asymptomatic incubation period than to the time to desiccation.

13653059, 2026, 6, Downloaded from https://bsppjournals.onlinelibrary.wiley.com/doi/10.1111/ppa.70322 by NICE, National Institute for Health and Care Excellence, Wiley Online Library on [18/11/2026]. See the Terms and Conditions (https://onlinelibrary.wiley.com/terms-and-conditions) on Wiley Online Library for rules of use; OA articles are governed by the applicable Creative Commons License

The increased proportion of asymptomatic individuals under longer incubation periods is particularly relevant for surveillance because visual inspection may fail to detect infected plants in the absence of conspicuous symptoms (Morelli et al. 2021). Thus, even where simulated prevalence is reduced under conditions associated with slower disease progression, a larger fraction of infections may remain asymptomatic and potentially less detectable.

3.2 | Simulation Scenarios

The maps in Figure 3 represented conditional model outputs following an assumed successful post-establishment spread and not probabilities of entry or establishment. The three scenarios representing British environmental conditions with three different dispersal kernels showed qualitatively consistent spatial patterns (Figure 3). However, the epidemic sizes resulting from entry of the pathogen at different locations varied among the three scenarios, with the number of infected trees decreasing with decreasing dispersal magnitude. Namely, the scenario combining both long- and short-distance dispersal resulted in the largest number of infected trees (GB_FullDispersal: Figure 3a), followed by the short-distance-only scenario (GB_Short: Figure 3b) and lastly by the scenario with reduced short-distance dispersal (GB_ShortReduced: Figure 3c). The relative difference in the number of infected trees among scenarios is shown in Figure S6. Nevertheless, all three British scenarios resulted in fewer infected trees than the Puglia scenario (Figures S6d and S7a).

The areas in which pathogen spread generated the largest epidemics were consistent across all three British scenarios, with the most notable hotspots located in southern and south-eastern England (Figure 3). Epidemic extent partially followed the underlying temperature gradient (Figures 3 and S2a), with greater spread observed in warmer areas. However, outbreak extent was also associated with host availability and the spatial continuity of susceptible host patches across the landscape (see next section). In contrast, cooler regions, including central and eastern Scotland, showed reduced outbreak extent despite the presence of potentially suitable hosts.

Spatial differences in outbreak extent among British scenarios were driven by variation in dispersal kernels and the configuration of susceptible host patches, with larger outbreaks occurring when introductions took place in counties containing major conurbations. Across all scenarios, the British eco-epidemiological setting generated prolonged epidemics with a high proportion of asymptomatic hosts at the end of the simulation period (Figure 4). Symptom progression was slower than in the Puglia scenario (Figure S7b), while extended host viability resulted in a longer potential infectious period.

3.3 | Landscape Metrics of the Infected Areas

Across all scenarios, the full GAM, including all spatial configuration metrics of susceptible cells, provided a better fit than the reduced candidate models. As dispersal distance decreased, the proportion of deviance explained by the spatial configuration of susceptible cells increased (Table 3), indicating that landscape configuration became increasingly important in determining simulated infection dynamics under more spatially constrained dispersal. Overall, larger susceptible patch area (PA), lower patch area coefficient of variation (PA_CV), shorter nearest neighbour distance (ENN), and lower patch density (PD, i.e., reduced fragmentation) were significantly associated with greater numbers of newly infected cells. These relationships were nonlinear, and their form varied among scenarios according to the assumed dispersal potential of the pathogen.

In the first scenario (GB_FullDispersal), patch area showed a positive association with the number of newly infected cells up to an apparent threshold size, beyond which the relationship levelled off. The high coefficient of variation (Table 3) indicated substantial patch-size heterogeneity, which was

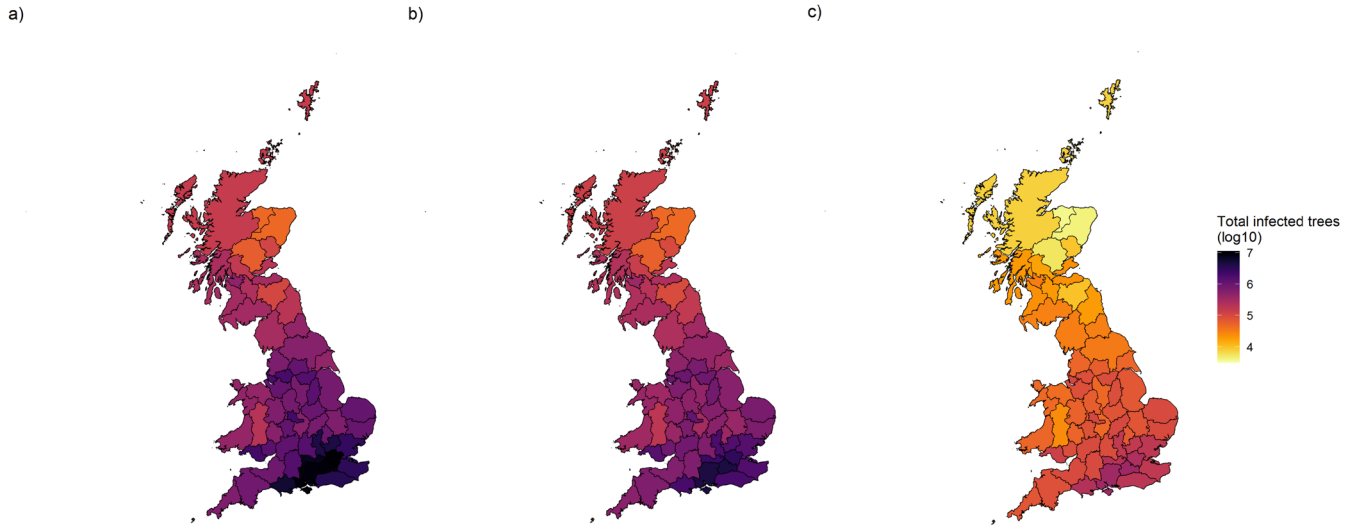

FIGURE 3 | Total number of infected trees ($\log_{10}$) for the scenarios listed in Table 2 for *Xylella fastidiosa* for Great Britain. County values represent the total number of infected trees at the end of the epidemic (16 years) when infection was introduced in the respective county. (a) Scenario GB_FullDispersal; (b) scenario GB_Short; (c) scenario GB_ShortReduced.

13653039, 2026, 6, Downloaded from https://bsppjournals.onlinelibrary.wiley.com/doi/10.1111/ppa.70322 by NICE, National Institute for Health and Care Excellence, Wiley Online Library on [18/11/2026]. See the Terms and Conditions (https://onlinelibrary.wiley.com/terms-and-conditions) on Wiley Online Library for rules of use; OA articles are governed by the applicable Creative Commons License

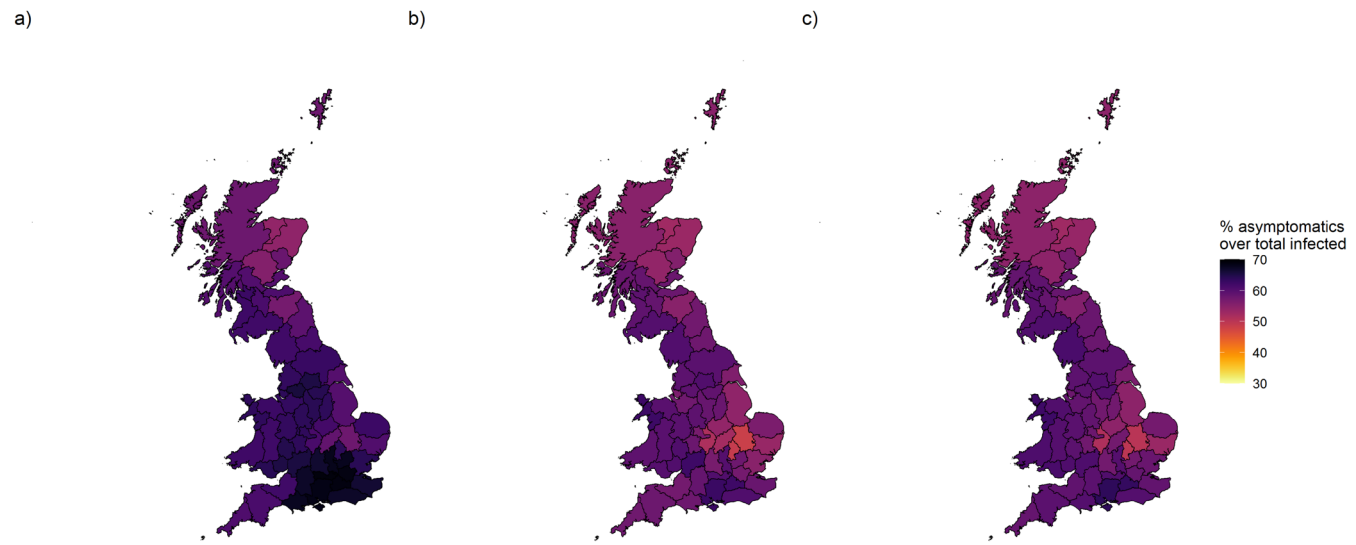

FIGURE 4 | Percentage of asymptomatic trees over total infected for the scenarios listed in Table 2 for *Xylella fastidiosa* for Great Britain. County values represent the overall proportion of asymptomatic trees at the end of the epidemic (16 years) when infection was introduced in the respective county. (a) Scenario GB_FullDispersal; (b) Scenario GB_Short; (c) Scenario GB_ShortReduced.

also associated with infection dynamics. ENN exhibited a fluctuating relationship with infection up to approximately 900 m, whereas values above this range showed a more linear positive association; although ENN was also highly variable, its variability had a weaker association with infection than patch area. Patch density displayed alternating associations up to approximately 5 patches/ha, beyond which increasing fragmentation was associated with reduced numbers of newly infected cells. In the scenario with exclusively short-distance dispersal (GB_Short), both patch area and its coefficient of variation followed a log-like relationship with infection, while associations with ENN and patch density were similar to those observed in the previous scenario. However, the apparent patch-density threshold beyond which fragmentation was associated with reduced infection was lower (approximately 2.5 patches/ha). Similarly, in the scenario with further reduced short-distance dispersal (GB_ShortReduced), patch area again showed a log-like relationship with infection, while the patch-density threshold associated with a marked reduction in infection was even lower (< 1 patch/ha).

Finally, according to the best-fitting GAMs, the metrics with the greatest contribution to explaining variation in the final number of infected cells differed among dispersal scenarios: patch size variability and patch density in scenario GB_FullDispersal; patch size, patch size variability, and patch density in scenario GB_Short (only short-distance dispersal); and patch size, patch size variability, ENN, and ENN variability in scenario GB_ShortReduced (reduced short-distance dispersal) (Table 3).

4 | Discussion

Our results suggested that, should *X. fastidiosa* enter and successfully establish in Great Britain, spread would likely occur at substantially lower rates than in Puglia. In an outbreak, the proportion of asymptomatic plants would most likely be higher than during the Puglian OQDS epidemic, consistent with experimental infections of European Salicaceae under temperate conditions (Casarin et al. 2022). Outbreaks initiated in areas with higher average summer temperatures, particularly southern and southeastern England, consistently produced larger outbreaks across dispersal scenarios. However, the spatial configuration of susceptible hosts also influenced landscape-scale spread, particularly at shorter dispersal distances. Because simulations began with an infected individual already present in a susceptible landscape, the model estimated potential post-establishment spread rather than the probability of entry, establishment or persistence. It therefore addressed how an established population could spread under British environmental and landscape conditions rather than explaining differences in epidemic occurrence among European regions.

Drawing on temperature-dependent bacterial growth experiments (Román-Écija et al. 2026) and published suitability assessments (EFSA et al. 2019; Godefroid, Cruaud, et al. 2022; Schneider et al. 2020), we assumed that British conditions are less favourable for pathogen growth than those in Puglia. The model therefore represented slower within-host colonisation and disease progression, including delayed symptom expression and extended desiccation time. Infection and disease development depend on interactions between bacterial strains and host species (Occhibove et al. 2020), but in the absence of sufficient British host-strain data we represented an effective average strain–host interaction. Lower temperatures and reduced hydric stress are generally associated with slower symptom development and lower transmissibility (Choi et al. 2013; Daugherty et al. 2017; de Pascali et al. 2019; Feil and Purcell 2001; McElrone et al. 2001; Lieth et al. 2011), while prolonged temperature-dependent asymptomatic periods are well documented in plant-pathogenic bacteria (e.g., Chang et al. 1992; Hayward 1974; Vidaver 1982) and fungal plant pathogens (e.g., Xu and Robinson 2000).

The stark contrast in modelled disease progression between the dry Mediterranean conditions of Puglia and the wet

13653039, 2026, 6, Downloaded from https://bsppjournals.onlinelibrary.wiley.com/doi/10.1111/ppa.70322 by NICE, National Institute for Health and Care Excellence, Wiley Online Library on [18/11/2026]. See the Terms and Conditions (https://onlinelibrary.wiley.com/terms-and-conditions) on Wiley Online Library for rules of use; OA articles are governed by the applicable Creative Commons License

TABLE 3 | Summary of generalised additive model (GAM) outputs for the total number of infected cells at the end of the epidemic of *Xylella fastidiosa* in Great Britain as a function of landscape metrics.

Scenario	*n*	Model	Variable	Deviance explained (%)
GB_FullDispersal	146,380	Full	PA	58.9
			PA_CV	
			ENN	
			ENN_CV	
			PD	
		Reduced	PA_CV	57.5
			PD	
GB_Short	139,917	Full	PA	82.0
			PA_CV	
			ENN	
			ENN_CV	
			PD	
		Reduced	PA	79.5
			PA_CV	
			PD	
GB_ShortReduced	87,518	Full	PA	90.0
			PA_CV	
			ENN	
			ENN_CV	
			PD	
		Reduced	PA	88.9
			PA_CV	
			ENN	
			ENN_CV	

Note: For each scenario, both the full model (including all selected explanatory variables) and the best-fitting reduced model (with a subset of explanatory variables) are reported. *n* indicates the number of simulations for which landscape metrics were calculated; this may differ from the total number of simulations reported in the Methods, as some entries of *Xylella fastidiosa* did not result in further spread in Great Britain. *p*-value was <0.0001 for each variable in every scenario.
Abbreviations: ENN, mean Euclidean nearest-neighbour distance between patches; ENN_CV, coefficient of variation of ENN; PA, mean patch area; PA_CV, coefficient of variation of patch area; PD, patch density.

temperate climate of Great Britain indicated that a high proportion of asymptomatic individuals is plausible in Britain. Although potentially less infectious, these plants may form a hidden reservoir and impede early detection, particularly where surveillance relies on visual inspection (Parnell et al. 2015). This could complicate detection and eradication efforts (Mastin et al. 2019), allowing prolonged undetected persistence across diverse host communities. Similar delays between introduction and disease recognition have been documented for *Phytophthora ramorum* and *Phytophthora kernoviae* (Denman et al. 2009) and ash dieback (*Hymenoscyphus fraxineus*; Combes et al. 2024). Asymptomatic infections could also provide a reservoir from which severe outbreaks develop in highly susceptible amplification hosts such as lavender and grapevine, which are relatively widespread in Great Britain and could have substantial ecological and economic impacts as a result. Evidence from Corsica demonstrates that long-standing infection in diverse symptomless hosts can sustain severe epidemics despite control efforts (Soubeyrand et al. 2018). Consequently, understanding the duration and infectiousness of the asymptomatic phase is important for estimating spread and designing surveillance and control strategies (Leclerc et al. 2014; Lee et al. 2015).

Beyond temperature, host spatial configuration was an important determinant of spread, particularly under the shorter dispersal scenarios (GB_Short and GB_ShortReduced) that are considered the most plausible given the current knowledge of potential British vectors. Some locations of entry generated unexpectedly large outbreaks despite comparatively lower temperature suitability, notably in northwest England, the West Midlands, southern Wales and, to a lesser extent, the north Midlands. These areas

13653059, 2026, 6, Downloaded from https://bsppjournals.onlinelibrary.wiley.com/doi/10.1111/ppa.70322 by NICE, National Institute for Health and Care Excellence, Wiley Online Library on [18/11/2026]. See the Terms and Conditions (https://onlinelibrary.wiley.com/terms-and-conditions) on Wiley Online Library for rules of use; OA articles are governed by the applicable Creative Commons License

contained larger and more connected patches of susceptible hosts (Figure S5), potentially associated with continuous broadleaved woodland and urban or suburban green spaces. This supports evidence that host connectivity, inter-plant distance and patch structure influence *X. fastidiosa* dispersal (Krugner et al. 2019; Santoiemma et al. 2019) and spread of plant pathogens more generally (Caraco et al. 2001; Papaïx et al. 2015). Variation in host spatial configuration may also affect host resistance evolution, as resistance can depend on host fragmentation (Jousimo et al. 2014), though this was beyond the scope of the study. Our results, partially reflecting the national gradient in summer temperatures (Figure S2a), also differed from correlative *Xylella* species-distribution models, which predicted greater suitability in Cornwall and along southern English and Welsh coasts (EFSA et al. 2019; Godefroid et al. 2019; Schneider et al. 2020; Figure 3 vs. Figure S8). This difference highlights the value of mechanistic models that account for transmission, host abundance and landscape structure in addition to climatic suitability (Raparelli et al. 2024). The higher suitability of southeastern England in our simulations is nevertheless consistent with projections of global *X. fastidiosa* distribution under climate change (Alqahtani et al. 2025). Unlike correlative suitability models, our mechanistic framework explicitly represented transmission and alternative dispersal mechanisms with associated transmission rates, which are key determinants of epidemic timing and magnitude (Giménez-Romero et al. 2023), alongside temperature, host abundance and spatial configuration.

Our present-day simulation should also be considered in the context of future climate change. A warming of approximately 2°C–3°C could increase thermal suitability for *X. fastidiosa* in currently marginal regions of Europe, potentially including parts of Great Britain, and increase transmission rates (Giménez-Romero et al. 2022). Such warming may also make establishment of some subspecies more viable in northern Europe. However, temperature change alone cannot be interpreted as a prediction of future establishment. Climate change will also modify host distributions and phenology, vector abundance and phenology, plant water status, landscape processes and overwintering persistence, potentially with opposing effects (Moralejo et al. 2026). In particular, changes in winter temperature could alter bacterial and vector survival in ways not represented here. Future assessments should therefore integrate temperature and precipitation with host phenology, vector ecology, plant water status and overwintering persistence rather than applying a uniform temperature increase to the present model. The relatively low spread rates predicted under current British conditions should consequently be regarded as a baseline rather than evidence that long-term risk is negligible. This is particularly relevant because climate and land-use change can promote vector-borne disease expansion (Swei et al. 2020), while *X. fastidiosa* has evolutionary potential that may increase pathogenicity (Sicard et al. 2018). Evidence that the bacterium can persist and potentially replicate under less favourable conditions further supports the need to consider these processes (Casarin et al. 2022; Landa et al. 2019; Sicard et al. 2018).

The spatiotemporal epidemiological dynamics captured by the model have implications for preparedness measures. Mechanistic, spatially explicit models such as ours can complement correlative suitability assessments by identifying where host abundance, connectivity, temperature and transmission interact to produce potentially large outbreaks. This can support risk-based surveillance rather than reliance on visual inspection alone (Hyatt-Twynam et al. 2017). The framework can also be adapted as new information becomes available, including data on vector responses to temperature and habitat characteristics (Avosani et al. 2022; Chapman et al. 2022; Godefroid, Morente, et al. 2022), and used to evaluate surveillance and control strategies under uncertainty (Cunniffe et al. 2014, 2015, 2016; Flores-García et al. 2026). In an emerging outbreak, such models can explore early epidemic dynamics (Thompson et al. 2018). This is particularly relevant for *X. fastidiosa*, for which substantial uncertainty remains outside currently affected regions and where existing models often focus on idealised outbreak conditions or known ecological niches (Mourou et al. 2025). The importance of representing ecological and spatial heterogeneity is also illustrated by modelling of the Puglian outbreak, where assuming homogeneous infection areas and ignoring abiotic and biotic heterogeneity affected epidemic dynamics and control effectiveness (Bozzo et al. 2022).

Despite these insights, the model is constrained by data limitations and simplifying assumptions that introduce both parameter and structural uncertainty. Within these constraints, the framework was designed to explore policy-relevant questions under a precautionary, 'worst-case scenario' set of assumptions, rather than to provide a prediction of realised outbreak dynamics. First, the host landscape represents potential susceptible biomass rather than epidemiologically weighted host competence. EFSA-listed hosts can differ substantially in susceptibility, bacterial multiplication, symptom expression and ability to support vector acquisition, but species-specific British host-strain data are largely unavailable. Host abundance and spatial configuration were therefore used to represent potential connectivity, while disease progression and transmission were represented using an effective average host–pathogen interaction. Potential hosts are likely to differ in their epidemiological contribution, with some acting predominantly as sinks and others as amplification hosts, although quantitative evidence is currently insufficient to classify most EFSA-listed hosts robustly across strains and environmental contexts (EFSA et al. 2019). Improved host inventories and experimental estimates of susceptibility, bacterial multiplication, symptom expression and vector acquisition would allow host competence to be represented explicitly.

Second, the temperature suitability parameterisation was subject to uncertainty because the temperature response was fitted to growth data from 12 *X. fastidiosa* strains representing four subspecies. Using the mean response avoids assuming a particular future pathway of entry, but also masks potentially important differences in thermal tolerance. Consequently, the model may underestimate thermal suitability for strains or subspecies that perform better than the fitted mean under cooler conditions, while overestimating it for less cold-tolerant strains. Strain- and subspecies-specific parameterisation could therefore alter the relative suitability of different British regions, but the available experimental evidence is currently insufficient to determine whether observed differences represent consistent subspecies-level responses rather than strain-level variation. Further experimental work is needed to quantify temperature responses across relevant strains, subspecies and host combinations. Mean summer temperature is another simplification

13653059, 2026, 6, Downloaded from https://bsppjournals.onlinelibrary.wiley.com/doi/10.1111/ppa.70322 by NICE, National Institute for Health and Care Excellence, Wiley Online Library on [18/11/2026]. See the Terms and Conditions (https://onlinelibrary.wiley.com/terms-and-conditions) on Wiley Online Library for rules of use; OA articles are governed by the applicable Creative Commons License

because bacterial multiplication, vector activity and transmission respond to finer temporal variation, including short periods of low temperature, diurnal variation and the cumulative duration of favourable conditions. Vector movement, phenology and transmission efficiency under British conditions are similarly uncertain. Future models would benefit from higher temporal-resolution temperature data combined with experimental and field observations of bacterial dynamics and vector ecology under temperate conditions.

Third, temperature suitability does not represent overwintering persistence or establishment. The model does not explicitly simulate winter cold-curing or temperature-driven bacterial mortality; therefore, favourable summer temperatures do not necessarily imply that infected plants remain epidemiologically viable until the following transmission season. The results should consequently be interpreted as potential transmission capacity conditional on infection being present, rather than as direct estimates of establishment probability. Cold curing has been demonstrated principally in the Pierce's disease–grapevine pathosystem (Lieth et al. 2011), whereas comparable quantitative evidence is lacking for other important host–strain combinations, including olive and the diverse potential British host community (EFSA et al. 2019). Applying a single cold-curing threshold across these systems would therefore introduce unsupported biological precision. Experimental data on survival over winter, cold-induced mortality and cold curing across relevant host–strain combinations are needed before these processes can be parameterised explicitly. A related limitation concerns the asymptomatic phase and its environmental scaling. The mean symptomless period was retained from White et al. (2020) as an effective parameter because comparable estimates for British host–strain combinations are unavailable, and its environmental scaling was represented through w_I. Similarly, w_D was explored over a plausible range because quantitative relationships between environmental conditions, plant hydric stress and disease progression remain poorly characterised. The model also did not explicitly represent seasonal host phenology or distinguish evergreen from deciduous hosts. This is particularly relevant in Great Britain, where many potential woody hosts are deciduous, unlike the evergreen olive system from which the symptomless-period parameter was derived. Uncertainty in the duration and infectiousness of the asymptomatic phase therefore affects epidemic development and the persistence of infectious material in the landscape. Future studies should quantify bacterial persistence, symptom development and transmission through dormancy and regrowth, and determine bacterial load, infectiousness and vector acquisition from asymptomatic plants across host–strain combinations. Such data would allow asymptomatic transmission to be represented more explicitly.

Finally, because simulations begin with an infected asymptomatic individual, the model did not simulate entry, establishment or long-term persistence. Nevertheless, the framework provides a structured means of identifying which biological uncertainties are most consequential for predicted spread and can therefore help prioritise future experimental work. In particular, empirical estimates of host competence, strain- and subspecies-specific thermal responses, vector ecology, host phenology and survival over winter can be progressively incorporated as they become available, allowing the framework and its predictions to be refined.

In conclusion, conditional on successful entry and establishment, our results indicated that *X. fastidiosa* could spread in Great Britain, but with substantially slower spread and smaller modelled epidemics than under the Puglian conditions represented here, suggesting the potential for correspondingly lower environmental damage. Temperature and host spatial configuration emerged as important determinants of outbreak size, with implications for risk-based surveillance, while prolonged asymptomatic infection could allow the pathogen to remain undetected and thus maintain infectious host material in the landscape, increasing the potential for subsequent spread. Great Britain therefore cannot be considered environmentally unsuitable for post-establishment spread. Rather, our results identified the environmental and landscape conditions under which a successful introduction could develop into a larger outbreak and provided a framework for evaluating surveillance and mitigation strategies, as well as changes in risk under future climate conditions.

Author Contributions

Flavia Occhibove: conceptualization, methodology, software, investigation, data curation, visualization, writing – original draft, writing – review and editing. **Daniel S. Chapman:** conceptualization, funding acquisition, methodology, software, supervision, validation, writing – review and editing. **Steven M. White:** conceptualization, funding acquisition, methodology, project administration, resources, supervision, writing – original draft, writing – review and editing.

Acknowledgements

We would like to thank all the partners of the BRIGIT consortium for the data informing model assumptions and parameterisation, and J. A. Navas-Cortés and M. Román-Écija for bacterium growth data.

Funding

This work was funded by UK Research and Innovation (UKRI) through the Strategic Priorities Fund (SPF), by a grant from the Biotechnology and Biological Sciences Research Council (BBSRC) (BB/S016325/1) with support from the Department for Environment, Food and Rural Affairs (Defra) and the Scottish Government (BB/S016325/1).

Conflicts of Interest

The authors declare no conflicts of interest.

Data Availability Statement

The data used to parameterise the model are available at the references provided (see Methods and Table 1). The code, input and parameter files used to generate the findings of this study are openly available in GitHub at https://github.com/flafflyfreak/GB_Xfspread.

References

Abatzoglou, J. T., S. Z. Dobrowski, S. A. Parks, and K. C. Hegewisch. 2018. "Terraclimate, a High-Resolution Global Dataset of Monthly Climate and Climatic Water Balance From 1958–2015." *Scientific Data* 5: 170191. https://doi.org/10.1038/sdata.2017.191.

Abboud, C., O. Bonnefon, E. Parent, and S. Soubeyrand. 2019. "Dating and Localizing an Invasion From Post-Introduction Data and a Coupled Reaction–Diffusion–Absorption Model." *Journal of Mathematical Biology* 79: 765–789. https://doi.org/10.1007/s00285-019-01376-x.

13653059, 2026, 6, Downloaded from https://bsppjournals.onlinelibrary.wiley.com/doi/10.1111/ppa.70322 by NICE, National Institute for Health and Care Excellence, Wiley Online Library on [18/11/2026]. See the Terms and Conditions (https://onlinelibrary.wiley.com/terms-and-conditions) on Wiley Online Library for rules of use; OA articles are governed by the applicable Creative Commons License

Allen, L. J. S. 1994. "Some Discrete-Time SI, SIR, and SIS Epidemic Models." *Mathematical Biosciences* 124: 83–105. https://doi.org/10.1016/0025-5564(94)90025-6.

Almeida, R. P. P., and L. Nunney. 2015. "How Do Plant Diseases Caused by *Xylella fastidiosa* Emerge?" *Plant Disease* 99: 1457–1467. https://doi.org/10.1094/PDIS-02-15-0159-FE.

Alqahtani, M. S. M., E. Ak, and S. M. H. Khalaf. 2025. "Projecting the Global Spread of *Xylella fastidiosa* Under Climate Change Using MaxEnt Modeling." *Scientific Reports* 15: 32460.

Avosani, S., C. Tattoni, V. Mazzoni, and M. Ciolli. 2022. "Occupancy and Detection of Agricultural Threats: The Case of *Philaenus spumarius*, European Vector of *Xylella fastidiosa*." *Agriculture, Ecosystems and Environment* 324: 107707. https://doi.org/10.1016/j.agee.2021.107707.

Bozzo, F., M. Frem, V. Fucilli, et al. 2022. "Landscape and Vegetation Patterns Zoning Is a Methodological Tool for Management Costs Implications due to *Xylella fastidiosa* Invasion." *Land* 11: 1105. https://doi.org/10.3390/land11071105.

Briscoe, N. J., J. Elith, R. Salguero-Gómez, et al. 2019. "Forecasting Species Range Dynamics With Process-Explicit Models: Matching Methods to Applications." *Ecology Letters* 22: 1940–1956. https://doi.org/10.1111/ele.13348.

Calderoni, F., A. Petrontino, M. Frem, V. Fucilli, and F. Bozzo. 2025. "Economic and Social Impacts of Olive Quick Decline Syndrome: Analysing Data From the Italian Farm Accountancy Network." *Plant Pathology* 74: 1010–1023. https://doi.org/10.1111/ppa.14069.

Caraco, T., M. C. Duryea, S. Glavanakov, W. Maniatty, and B. K. Szymanski. 2001. "Host Spatial Heterogeneity and the Spread of Vector-Borne Infection." *Theoretical Population Biology* 59: 185–206. https://doi.org/10.1006/tpbi.2000.1517.

Casarin, N., S. Hasbroucq, L. Pesenti, et al. 2022. "Salicaceae as Potential Host Plants of *Xylella fastidiosa* in European Temperate Regions." *European Journal of Plant Pathology* 165: 489–507. https://doi.org/10.1007/s10658-022-02622-7.

Cendoya, M., J. Martínez-Minaya, V. Dalmau, et al. 2020. "Spatial Bayesian Modeling Applied to the Surveys of *Xylella fastidiosa* in Alicante (Spain) and Apulia (Italy)." *Frontiers in Plant Science* 11: 1204. https://doi.org/10.3389/fpls.2020.01204.

Chang, R. J., S. M. Ries, and J. K. Pataky. 1992. "Effects of Temperature, Plant Age, Inoculum Concentration, and Cultivar on the Incubation Period and Severity of Bacterial Canker of Tomato." *Plant Disease* 76: 1150–1155.

Chapman, D. S., S. A'Hara, S. Broadmeadow, et al. 2022. *Improving Knowledge of Xylella fastidiosa Vector Ecology: Modelling Vector Occurrence and Abundance in the Wider Landscape in Scotland: Project Final Report*. PHC2020/04. Scotland's Centre of Expertise for Plant Health (PHC).

Chapman, D. S., F. Occhibove, J. M. Bullock, P. S. A. Beck, J. A. Navas-Cortes, and S. M. White. 2025. "Modelling Plant Disease Spread and Containment: Simulation and Approximate Bayesian Computation for *Xylella fastidiosa* in Puglia, Italy." *PLoS Computational Biology* 21: e1013539. https://doi.org/10.1371/journal.pcbi.1013539.

Chapman, D. S., B. V. Purse, H. E. Roy, and J. M. Bullock. 2017. "Global Trade Networks Determine the Distribution of Invasive Non-Native Species." *Global Ecology and Biogeography* 26: 907–917. https://doi.org/10.1111/geb.12599.

Choi, H. K., A. Iandolino, F. G. Da Silva, and D. R. Cook. 2013. "Water Deficit Modulates the Response of *Vitis vinifera* to the Pierce's Disease Pathogen *Xylella fastidiosa*." *Molecular Plant–Microbe Interactions* 26: 643–657. https://doi.org/10.1094/MPMI-09-12-0217-R.

Colella, C., R. Carradore, and A. Cerroni. 2019. "Problem Setting and Problem Solving in the Case of Olive Quick Decline Syndrome in Apulia, Italy: A Sociological Approach." *Phytopathology* 109: 187–199. https://doi.org/10.1094/PHYTO-07-18-0247-FI.

Combes, M., J. Webber, and L. Boddy. 2024. "Current Understanding and Future Prospects for Ash Dieback Disease With a Focus on Britain." *Forestry* 97: 678–691. https://doi.org/10.1093/forestry/cpae040.

Condeso, T. E., and R. K. Meentemeyer. 2007. "Effects of Landscape Heterogeneity on the Emerging Forest Disease Sudden Oak Death." *Journal of Ecology* 95: 364–375. https://doi.org/10.1111/j.1365-2745.2006.01206.x.

Cornara, D., M. Morente, A. Markheiser, et al. 2019. "An Overview on the Worldwide Vectors of *Xylella fastidiosa*." *Entomologia Generalis* 39: 157–181. https://doi.org/10.1127/entomologia/2019/0811.

Crowther, T. W., H. B. Glick, K. R. Covey, et al. 2015. "Mapping Tree Density at a Global Scale." *Nature* 525: 201–205. https://doi.org/10.1038/nature14967.

Cunniffe, N. J., F. F. Laranjeira, F. M. Neri, R. E. DeSimone, and C. A. Gilligan. 2014. "Cost-Effective Control of Plant Disease When Epidemiological Knowledge Is Incomplete: Modelling Bahia Bark Scaling of Citrus." *PLoS Computational Biology* 10: e1003753. https://doi.org/10.1371/journal.pcbi.1003753.

Cunniffe, N. J., D. M. Rizzo, R. K. Meentemeyer, R. C. Cobb, and C. A. Gilligan. 2016. "Modeling When, Where, and How to Manage a Forest Epidemic, Motivated by Sudden Oak Death in California." *Proceedings of the National Academy of Sciences of the United States of America* 113: 5640–5645. https://doi.org/10.1073/pnas.1602153113.

Cunniffe, N. J., R. O. J. H. Stutt, R. E. DeSimone, T. R. Gottwald, and C. A. Gilligan. 2015. "Optimising and Communicating Options for the Control of Invasive Plant Disease When There Is Epidemiological Uncertainty." *PLoS Computational Biology* 11: e1004211. https://doi.org/10.1371/journal.pcbi.1004211.

Daugherty, M. P., A. R. Zeilinger, and R. P. P. Almeida. 2017. "Conflicting Effects of Climate and Vector Behavior on the Spread of a Plant Pathogen." *Phytobiomes Journal* 1: 46–53. https://doi.org/10.1094/PBIOMES-01-17-0004-R.

de Pascali, M., M. Vergine, E. Sabella, et al. 2019. "Molecular Effects of *Xylella fastidiosa* and Drought Combined Stress in Olive Trees." *Plants* 8: 437. https://doi.org/10.3390/plants8110437.

Defra. 2020. "Rapid Pest Risk Analysis (PRA) for: *Xylella fastidiosa*." https://pra.eppo.int/pra/c8b461a8-3e0c-4c67-abe0-73d5149ead91.

Denman, S., S. A. Kirk, E. Moralejo, and J. F. Webber. 2009. "*Phytophthora ramorum* and *Phytophthora kernoviae* on Naturally Infected Asymptomatic Foliage." *EPPO Bulletin* 39: 105–111. https://doi.org/10.1111/j.1365-2338.2009.02243.x.

Dilts, T. E., P. J. Weisberg, C. M. Dencker, and J. C. Chambers. 2015. "Functionally Relevant Climate Variables for Arid Lands: A Climatic Water Deficit Approach for Modelling Desert Shrub Distributions." *Journal of Biogeography* 42: 1986–1997. https://doi.org/10.1111/jbi.12561.

EFSA. 2025. "Update of the *Xylella* spp. Host Plant Database – Systematic Literature Search up to 30 June 2024." *EFSA Journal* 23: e9241.

EFSA, C. Bragard, K. Dehnen-Schmutz, et al. 2019. "EFSA Panel on Plant Health (PLH). Update of the Scientific Opinion on the Risks to Plant Health Posed by *Xylella fastidiosa* in the EU Territory." *EFSA Journal* 17: e05665.

EPPO. 2025. "*Xylella fastidiosa*. EPPO Datasheets on Pests Recommended for Regulation." Accessed November 28, 2025. https://gd.eppo.int.

EU. 2015. "Commission Implementing Decision (EU) 2015/789 of 18 May 2015 as Regards Measures to Prevent the Introduction Into and the Spread Within the Union of *Xylella fastidiosa* (Wells et al.) (Notified Under Document C(2015) 3415)." https://eur-lex.europa.eu/eli/dec_impl/2015/789/oj/eng.

Feil, H., and A. H. Purcell. 2001. "Temperature-Dependent Growth and Survival of *Xylella fastidiosa* In Vitro and in Potted Grapevines."

13653059, 2026, 6, Downloaded from https://bsppjournals.onlinelibrary.wiley.com/doi/10.1111/ppa.70322 by NICE, National Institute for Health and Care Excellence, Wiley Online Library on [18/11/2026]. See the Terms and Conditions (https://onlinelibrary.wiley.com/terms-and-conditions) on Wiley Online Library for rules of use; OA articles are governed by the applicable Creative Commons License

Plant Disease 85: 1230–1234. https://doi.org/10.1094/PDIS.2001.85.12.1230.

Flores-García, A., J. Y. Dobson, E. S. Fonfría, D. García-García, J. García-Martínez, and C. Bordehore. 2026. "A Dynamic Model of the *Xylella fastidiosa* Pathosystem as a Tool to Optimize Management Scenarios: An Example Using the Almond Tree." *Ecological Modelling* 513: 111430. https://doi.org/10.1016/j.ecolmodel.2025.111430.

Giménez-Romero, À., J. Galván, M. Montesinos, et al. 2022. "Global Predictions for the Risk of Establishment of Pierce's Disease of Grapevines." *Communications Biology* 5: 1389. https://doi.org/10.1038/s42003-022-04358-w.

Giménez-Romero, À., E. Moralejo, and M. A. Matías. 2023. "A Compartmental Model for *Xylella fastidiosa* Diseases With Explicit Vector Seasonal Dynamics." *Phytopathology* 113: 1686–1696. https://doi.org/10.1094/PHYTO-11-22-0428-V.

Godefroid, M., A. Cruaud, J. C. Streito, J. Y. Rasplus, and J. P. Rossi. 2019. "*Xylella fastidiosa*: Climate Suitability of European Continent." *Scientific Reports* 9: 8844. https://doi.org/10.1038/s41598-019-45365-y.

Godefroid, M., A. Cruaud, J. C. Streito, J. Y. Rasplus, and J. P. Rossi. 2022. "Forecasting Future Range Shifts of *Xylella fastidiosa* Under Climate Change." *Plant Pathology* 71: 1839–1848. https://doi.org/10.1111/ppa.13637.

Godefroid, M., M. Morente, T. Schartel, et al. 2022. "Climate Tolerances of *Philaenus spumarius* Should Be Considered in Risk Assessment of Disease Outbreaks Related to *Xylella fastidiosa*." *Journal of Pest Science* 95: 855–868. https://doi.org/10.1007/s10340-021-01413-z.

Gonçalves, F. P., E. S. Stuchi, S. A. Lourenço, A. B. Kriss, T. R. Gottwald, and L. Amorim. 2014. "The Effect of Irrigation on Development of Citrus Variegated Chlorosis Symptoms." *Crop Protection* 57: 8–14. https://doi.org/10.1016/j.cropro.2013.11.016.

Gould, A. B., and J. H. Lashomb. 2005. "Bacterial Leaf Scorch of Shade Trees." APSnet Features Online. https://www.apsnet.org/edcenter/apsnetfeatures/Pages/BacterialLeafScorch.aspx.

Hayward, A. C. 1974. "Latent Infections by Bacteria." *Annual Review of Phytopathology* 12: 87–97. https://doi.org/10.1146/annurev.py.12.090174.000511.

Hesselbarth, M. H. K., M. Sciaini, K. A. With, K. Wiegand, and J. Nowosad. 2019. "Landscapemetrics: An Open-Source R Tool to Calculate Landscape Metrics." *Ecography* 42: 1648–1657. https://doi.org/10.1111/ecog.04617.

Hill, M. O., C. D. Preston, and D. B. Roy. 2004. *PLANTATT—Attributes of British and Irish Plants: Status, Size, Life History, Geography and Habitats*. Centre for Ecology and Hydrology.

Hogenhout, S. A., D. S. Chapman, F. Occhibove, et al. 2022. *BRIGIT: Surveillance and Response Capacity for Xylella fastidiosa*. John Innes Centre/BBSRC. https://www.jic.ac.uk/brigit/.

Hyatt-Twynam, S. R., S. Parnell, R. O. J. H. Stutt, T. R. Gottwald, C. A. Gilligan, and N. J. Cunniffe. 2017. "Risk-Based Management of Invading Plant Disease." *New Phytologist* 214: 1317–1329. https://doi.org/10.1111/nph.14488.

IPSP-CNR, CRSFA Locorotondo, Università di Torino DISAFA, et al. 2019. *Collection of Data and Information on Biology and Control of Vectors of Xylella fastidiosa*. EFSA Supporting Publications.

Jousimo, J., A. J. M. Tack, O. Ovaskainen, et al. 2014. "Ecological and Evolutionary Effects of Fragmentation on Infectious Disease Dynamics." *Science* 344: 1289–1293. https://doi.org/10.1126/science.1253621.

Kottelenberg, D., L. Hemerik, M. Saponari, and W. van der Werf. 2021. "Shape and Rate of Movement of the Invasion Front of *Xylella fastidiosa* spp. *pauca* in Puglia." *Scientific Reports* 11: 1061. https://doi.org/10.1038/s41598-020-79279-x.

Krugner, R., M. S. Sisterson, E. A. Backus, L. P. Burbank, and R. A. Redak. 2019. "Sharpshooters: A Review of What Moves *Xylella fastidiosa*." *Austral Entomology* 58: 248–267. https://doi.org/10.1111/aen.12397.

Kyrkou, I., T. Pusa, L. Ellegaard-Jensen, M. F. Sagot, and L. H. Hansen. 2018. "Pierce's Disease of Grapevines: A Review of Control Strategies and an Outline of an Epidemiological Model." *Frontiers in Microbiology* 9: 2141. https://doi.org/10.3389/fmicb.2018.02141.

Landa, B. B., A. I. Castillo, A. Giampetruzzi, et al. 2019. "Multiple Intercontinental Introductions Associated With the Emergence of a Plant Pathogen in Europe." *Applied and Environmental Microbiology* 86: e01521-19.

Leclerc, M., T. Doré, C. A. Gilligan, P. Lucas, and J. A. N. Filipe. 2014. "Estimating the Delay Between Host Infection and Disease (Incubation Period) and Assessing Its Significance to the Epidemiology of Plant Diseases." *PLoS One* 9: e86568. https://doi.org/10.1371/journal.pone.0086568.

Lee, J. A., S. E. Halbert, W. O. Dawson, C. J. Robertson, J. E. Keesling, and B. H. Singer. 2015. "Asymptomatic Spread of Huanglongbing and Implications for Disease Control." *Proceedings of the National Academy of Sciences of the United States of America* 112: 7605–7610. https://doi.org/10.1073/pnas.1508253112.

Lieth, J. H., M. M. Meyer, K. H. Yeo, and B. C. Kirkpatrick. 2011. "Modeling Cold Curing of Pierce's Disease in *Vitis vinifera* "Pinot Noir" and "Cabernet Sauvignon" Grapevines in California." *Phytopathology* 101: 1492–1500. https://doi.org/10.1094/PHYTO-08-10-0207.

Loconsole, G., O. Potere, D. Boscia, et al. 2014. "Detection of *Xylella fastidiosa* in Olive Trees by Molecular and Serological Methods." *Journal of Plant Pathology* 96: 7–14. https://doi.org/10.4454/JPP.V96I1.041.

Martinetti, D., and S. Soubeyrand. 2019. "Identifying Lookouts for Epidemio-Surveillance: Application to the Emergence of *Xylella fastidiosa* in France." *Phytopathology* 109: 265–276. https://doi.org/10.1094/PHYTO-07-18-0237-FI.

Mastin, A. J., F. van den Bosch, F. van den Berg, and S. R. Parnell. 2019. "Quantifying the Hidden Costs of Imperfect Detection for Early Detection Surveillance." *Philosophical Transactions of the Royal Society B* 374: 20180261. https://doi.org/10.1098/rstb.2018.0261.

McElrone, A. J., J. L. Sherald, and I. N. Forseth. 2001. "Effects of Water Stress on Symptomatology and Growth of *Parthenocissus quinquefolia* Infected by *Xylella fastidiosa*." *Plant Disease* 85: 1160–1164. https://doi.org/10.1094/pdis.2001.85.11.1160.

Moralejo, E., M. Saponari, D. Boscia, and B. B. Landa. 2026. "Emerging Risk of *Xylella fastidiosa* in Europe Under Global Change." *Biological Invasions* 28: 162. https://doi.org/10.1007/s10530-026-03869-5.

Morelli, M., J. M. García-Madero, Á. Jos, et al. 2021. "*Xylella fastidiosa* in Olive: A Review of Control Attempts and Current Management." *Microorganisms* 9: 1771. https://doi.org/10.3390/microorganisms9081771.

Mourou, M., G. Incampo, M. Carlucci, et al. 2025. "Insight Into Biological Strategies and Main Challenges to Control the Phytopathogenic Bacterium *Xylella fastidiosa*." *Frontiers in Plant Science* 16: 1608687. https://doi.org/10.3389/fpls.2025.1608687.

Occhibove, F., D. S. Chapman, A. J. Mastin, et al. 2020. "Eco-Epidemiological Uncertainties of Emerging Plant Diseases: The Challenge of Predicting *Xylella fastidiosa* Dynamics in Novel Environments." *Phytopathology* 110: 1740–1750. https://doi.org/10.1094/PHYTO-03-20-0098-RVW.

Papaïx, J., J. J. Burdon, J. Zhan, and P. H. Thrall. 2015. "Crop Pathogen Emergence and Evolution in Agro-Ecological Landscapes." *Evolutionary Applications* 8: 385–402. https://doi.org/10.1111/eva.12251.

Parnell, S., T. R. Gottwald, N. J. Cunniffe, V. Alonso Chavez, and F. van den Bosch. 2015. "Early Detection Surveillance for an Emerging Plant

13653059, 2026, 6, Downloaded from https://bsppjournals.onlinelibrary.wiley.com/doi/10.1111/ppa.70322 by NICE, National Institute for Health and Care Excellence, Wiley Online Library on [18/11/2026]. See the Terms and Conditions (https://onlinelibrary.wiley.com/terms-and-conditions) on Wiley Online Library for rules of use; OA articles are governed by the applicable Creative Commons License

Pathogen: A Rule of Thumb to Predict Prevalence at First Discovery." *Proceedings of the Royal Society B: Biological Sciences* 282: 20151478. https://doi.org/10.1098/rspb.2015.1478.

Purcell, A. 2013. "Paradigms: Examples From the Bacterium *Xylella fastidiosa*." *Annual Review of Phytopathology* 51: 339–356. https://doi.org/10.1146/annurev-phyto-082712-102325.

R Core Team. 2024. *R: A Language and Environment for Statistical Computing*. R Foundation for Statistical Computing. https://www.R-project.org/.

Raparelli, E., S. Bajocco, F. Ginaldi, and G. Fila. 2024. "Mapping the Science Around *Xylella fastidiosa*: An Update After the Outbreak on Italian Olive Groves." *European Journal of Agronomy* 159: 127250. https://doi.org/10.1016/j.eja.2024.127250.

Rapicavoli, J., B. Ingel, B. Blanco-Ulate, D. Cantu, and C. Roper. 2018. "*Xylella fastidiosa*: An Examination of a Re-Emerging Plant Pathogen." *Molecular Plant Pathology* 19: 786–800. https://doi.org/10.1111/mpp.12585.

Robinson, E. L., E. M. Blyth, D. B. Clark, E. Comyn-Platt, and A. C. Rudd. 2020. *Climate Hydrology and Ecology Research Support System Meteorology Dataset for Great Britain (1961–2017) [CHESS-Met]*. NERC Environmental Information Data Centre.

Román-Écija, M., B. B. Landa, L. Testi, and J. A. Navas-Cortés. 2026. "Thermal Dynamics of Xylem and Soil-Root Temperatures in Olive and Almond Trees and Their Relationship With Air Temperature." *Agronomy* 16: 102. https://doi.org/10.3390/agronomy16010102.

Roper, C., C. Castro, and B. Ingel. 2019. "*Xylella fastidiosa*: Bacterial Parasitism With Hallmarks of Commensalism." *Current Opinion in Plant Biology* 50: 140–147. https://doi.org/10.1016/j.pbi.2019.05.005.

Rowland, C., D. Morton, L. Carrasco Tornero, G. McShane, A. O'Neil, and C. Wood. 2015. *Land Cover Map 2015 (25m Raster)*. NERC Environmental Information Data Centre. https://doi.org/10.5285/47f053a0-e34f-4534-a843-76f0a0998a2f.

Santoiemma, G., G. Tamburini, F. Sanna, N. Mori, and L. Marini. 2019. "Landscape Composition Predicts Distribution of *Philaenus spumarius*, Vector of *Xylella fastidiosa*, in Olive Groves." *Journal of Pest Science* 92: 1101–1109.

Saponari, M., D. Boscia, F. Nigro, and G. P. Martelli. 2013. "Identification of DNA Sequences Related to *Xylella fastidiosa* in Oleander, Almond and Olive Trees Exhibiting Leaf Scorch Symptoms in Apulia (Southern Italy)." *Journal of Plant Pathology* 95: 668. https://doi.org/10.4454/JPP.V95I3.035.

Saponari, M., A. Giampetruzzi, G. Loconsole, D. Boscia, and P. Saldarelli. 2019. "*Xylella fastidiosa* in Olive in Apulia: Where We Stand." *Phytopathology* 109: 175–186. https://doi.org/10.1094/PHYTO-08-18-0319-FI.

Schneider, K., W. Van der Werf, M. Cendoya, et al. 2020. "Impact of *Xylella fastidiosa* Subspecies *pauca* in European Olives." *Proceedings of the National Academy of Sciences of the United States of America* 117: 9250–9259. https://doi.org/10.1073/pnas.1912206117.

Sicard, A., A. R. Zeilinger, M. Vanhove, et al. 2018. "*Xylella fastidiosa*: Insights Into an Emerging Plant Pathogen." *Annual Review of Phytopathology* 56: 181–202. https://doi.org/10.1146/annurev-phyto-080417-045849.

Soubeyrand, S., P. de Jerphanion, O. Martin, et al. 2018. "Inferring Pathogen Dynamics From Temporal Count Data: The Emergence of *Xylella fastidiosa* in France Is Probably Not Recent." *New Phytologist* 219: 824–836. https://doi.org/10.1111/nph.15177.

Strona, G., C. J. Carstens, and P. S. A. Beck. 2017. "Network Analysis Reveals Why *Xylella fastidiosa* Will Persist in Europe." *Scientific Reports* 7: 71. https://doi.org/10.1038/s41598-017-00077-z.

Swei, A., L. I. Couper, L. L. Coffey, D. Kapan, and S. Bennett. 2020. "Patterns, Drivers, and Challenges of Vector-Borne Disease Emergence." *Vector-Borne and Zoonotic Diseases* 20: 159–170. https://doi.org/10.1089/vbz.2018.2432.

Thompson, R. N., C. A. Gilligan, and N. J. Cunniffe. 2018. "Control Fast or Control Smart: When Should Invading Pathogens Be Controlled?" *PLoS Computational Biology* 14: e1006014. https://doi.org/10.1371/journal.pcbi.1006014.

Tumber, K. P., J. M. Alston, and K. Fuller. 2014. "Pierce's Disease Costs California $104 Million Per Year." *California Agriculture* 68: 20–29. https://doi.org/10.3733/ca.v068n01p20.

UKCEH. 2016. *UKCEH Land Cover Plus: Crops*. UK Centre for Ecology and Hydrology. https://www.ceh.ac.uk/crops2015.

Vicente-Serrano, S. M., C. Gouveia, J. J. Camarero, et al. 2013. "Response of Vegetation to Drought Time-Scales Across Global Land Biomes." *Proceedings of the National Academy of Sciences of the United States of America* 110: 52–57. https://doi.org/10.1073/pnas.1207068110.

Vidaver, A. K. 1982. "The Plant Pathogenic Corynebacteria." *Annual Review of Microbiology* 36: 495–517. https://doi.org/10.1146/annurev.mi.36.100182.002431.

White, S. M., J. M. Bullock, D. A. P. Hooftman, and D. S. Chapman. 2017. "Modelling the Spread and Control of *Xylella fastidiosa* in the Early Stages of Invasion in Apulia, Italy." *Biological Invasions* 19: 1825–1837. https://doi.org/10.1007/s10530-017-1393-5.

White, S. M., J. A. Navas-Cortés, J. M. Bullock, D. Boscia, and D. S. Chapman. 2020. "Estimating the Epidemiology of Emerging *Xylella fastidiosa* Outbreaks in Olives." *Plant Pathology* 69: 1403–1413. https://doi.org/10.1111/ppa.13238.

Wood, S. N. 2011. "Fast Stable Restricted Maximum Likelihood and Marginal Likelihood Estimation of Semiparametric Generalized Linear Models." *Journal of the Royal Statistical Society. Series B, Statistical Methodology* 73: 3–36. https://doi.org/10.1111/j.1467-9868.2010.00749.x.

Xu, X.-M., and J. D. Robinson. 2000. "Effects of Temperature on the Incubation and Latent Periods of Hawthorn Powdery Mildew (*Podosphaera clandestina*)." *Plant Pathology* 49: 791–797. https://doi.org/10.1046/j.1365-3059.2000.00520.x.

Yates, K. L., P. J. Bouchet, M. J. Caley, et al. 2018. "Outstanding Challenges in the Transferability of Ecological Models." *Trends in Ecology and Evolution* 33: 790–802. https://doi.org/10.1016/j.tree.2018.08.001.

Supporting Information

Additional supporting information can be found online in the Supporting Information section. **Figure S1:** In vitro temperature-dependent growth curves for 12 *Xylella fastidiosa* strains representing four subspecies (*fastidiosa*, *multiplex*, *pauca*, and *sandyi*; grey dashed lines) and the fitted average growth curve (black solid line, equation: $y = 0.00016x^3 - 0.00317x^2 + 0.02062x - 0.04049$) across the full British summer temperature range. Grey solid lines indicate ± standard deviation. See Table 1 and Model Structure section for the estimation methodology of the temperature factor (C). **Figure S2:** (a) Temperature scaling factor (C) averaged by county; (b) tree density per county estimated from Crowther et al. (2015); (c) vegetation cover averaged by county using mean NDVI from MOD13Q1 16-day 250 m resolution. **Figure S3:** (a) Map of total susceptible areas and (b) seeding locations (152,923 points). Colours indicate different counties. **Figure S4:** Example of potential spatial spread of a *Xylella fastidiosa* epidemic front from a single simulation. Epidemic extent (coloured polygons) is shown after 4, 6, 10 and 16 years by connecting leading edges of infected cells with convex hulls. Black cross indicates entry location; grey areas represent susceptible zones where the pathogen can spread. **Figure S5:** Landscape metrics of estimated susceptible areas (200 × 200 m grid cells) at county level. Patches consist of adjacent cells (connected horizontally, vertically, and/or diagonally). Metrics include (a) total susceptible area (ha); (b) number of patches (NP); (c) patch density per hectare (PD); (d) mean patch area (PA, ha); (e) mean Euclidean nearest-neighbour

13653059, 2026, 6, Downloaded from https://bsppjournals.onlinelibrary.wiley.com/doi/10.1111/ppa.70322 by NICE, National Institute for Health and Care Excellence, Wiley Online Library on [18/11/2026]. See the Terms and Conditions (https://onlinelibrary.wiley.com/terms-and-conditions) on Wiley Online Library for rules of use; OA articles are governed by the applicable Creative Commons License

distance between patches (ENN, m); (f) patch cohesion index (higher values indicate greater aggregation). **Figure S6:** Differences in total infected trees at the end of simulations (Figure 3) among scenarios in Table 2: (a) GB_FullDispersal—GB_Short; (b) GB_FullDispersal—GB_ShortReduced; (c) GB_Short—GB_ShortReduced; (d) Puglia—GB_FullDispersal. In (d), grey areas indicate non-simulated cells, as the Puglia scenario was run only for a subset of the Great Britain spatial extent. Legends represent infected trees ($\log_{10}$). **Figure S7:** (a) Total number of infected trees ($\log_{10}$) and (b) percentage of asymptomatic trees over total infected for the Puglia scenario (see Table 2). County values represent total infected trees and overall proportion of asymptomatic trees at the end of the epidemic (16 years) when infection was introduced in that county. Grey areas indicate non-simulated cells, as the Puglia scenario was run only for a subset of the Great Britain spatial extent. **Figure S8:** *Xylella fastidiosa* suitability value averaged by county, scaled from Schneider et al. (2020) so that the Puglia infection zone equals 1. **Table S1:** Descriptive statistics of climatic water deficit (mm H_2O) for Great Britain and Puglia (*Xylella fastidiosa* infected zone) over 1980–2015 (Abatzoglou et al. 2018). **Table S2:** Statistics of *Xylella fastidiosa* suitability values for Great Britain (Schneider et al. 2020).

13653059, 2026, 6, Downloaded from https://bsppjournals.onlinelibrary.wiley.com/doi/10.1111/ppa.70322 by NICE, National Institute for Health and Care Excellence, Wiley Online Library on [18/11/2026]. See the Terms and Conditions (https://onlinelibrary.wiley.com/terms-and-conditions) on Wiley Online Library for rules of use; OA articles are governed by the applicable Creative Commons License